EFFECTS OF SALT FORMATION ON THE CHEMICAL ENVIRONMENT OF DRIP SHIELDS AND WASTE PACKAGES AT THE PROPOSED NUCLEAR WASTE REPOSITORY AT YUCCA MOUNTAIN, NEVADA

Prepared for

U.S. Nuclear Regulatory Commission
Contract NRC–02–97–009

Prepared by

Roberto T. Pabalan
Leitai Yang
Lauren B. Browning

Center for Nuclear Waste Regulatory Analyses
San Antonio, Texas

May 2002

301 - - - Q200205090003

Effects of Salt Formation on the Chemical Environment of Drip Shields and Waste Packages at the Proposed Nuclear Waste Repository at Yucca Mountain, Nevada

EFFECTS OF SALT FORMATION ON THE CHEMICAL ENVIRONMENT OF DRIP SHIELDS AND WASTE PACKAGES AT THE PROPOSED NUCLEAR WASTE REPOSITORY AT YUCCA MOUNTAIN, NEVADA

Prepared for

U.S. Nuclear Regulatory Commission
Contract NRC–02–97–009

Prepared by

Roberto T. Pabalan
Lietai Yang
Lauren Browning

Center for Nuclear Waste Regulatory Analyses
San Antonio, Texas

May 2002

ABSTRACT

A key attribute of the U.S. Department of Energy (DOE) safety strategy for the proposed high-level waste repository at Yucca Mountain, Nevada, is the long life of waste packages and drip shields. Aside from failures by potential mechanical disruption, aqueous corrosion is expected to be the primary degradation process limiting the life of the waste package and drip shield. The type, rate, and duration of drip shield and waste package corrosion that may occur in a repository are dependent on water chemistry and temperature. In a hot repository setting, evaporation processes could increase the aqueous concentrations of chloride, fluoride, and other ions and lead to the accumulation of multicomponent salt deposits on drip shield and waste package surfaces. Inorganic salts are generally hygroscopic and will absorb moisture from humid air, generating small volumes of potentially corrosive brines.

This report describes the results of modeling and experimental studies bearing on the plausible range of deleterious chemical conditions that may occur on the drip shield and waste package surfaces. Thermodynamic modeling was conducted to evaluate the effect of salt formation on the chemical environment of drip shields and waste packages at the proposed Yucca Mountain repository. The deliquescence behavior of salt mixtures was evaluated using thermodynamic considerations and compared with that of single salts. The chemical evolution of Yucca Mountain groundwaters was evaluated to determine the types of brines and salt mixtures that could form by evaporation processes. To support the thermodynamic calculations, experimental determinations of the deliquescence points of salt mixtures also were performed. In addition, the relative values of ionic conductivity of various salts were measured because aqueous corrosion requires the presence of an electrolyte conductive to ionic species.

The results of thermodynamic calculations and experimental measurements support literature data that show the deliquescence points of salt mixtures are lower than those of individual salts. Thermodynamic analyses indicate that mixtures comprising NaCl and KCl salts have higher deliquescence points than pure $NaNO_3$, but measured values for mixtures of NaCl, $NaNO_3$, and KNO_3 are significantly lower than for pure $NaNO_3$. Additional thermodynamic analyses and experimental measurements show that mixtures containing magnesium and calcium have much lower deliquescence points than pure $NaNO_3$. The current DOE (CRWMS M&O, 2000a) analysis of the chemical environment on the surface of drip shields and waste packages is based on the deliquescence behavior of pure $NaNO_3$. Salt mixtures likely to form on drip shield and waste package surfaces will have lower deliquescence points compared to pure $NaNO_3$. Thus, the onset of aqueous corrosion of the drip shield and waste package may be earlier and its duration may be longer than that assumed by DOE. In addition, because deliquescence points generally decrease with increasing temperature, a lower deliquescence point implies that formation of a corrosive brine and possible initiation of aqueous corrosion may occur at a temperature higher than is assumed based on the deliquescence behavior of $NaNO_3$.

Thermodynamic simulations show that some Yucca Mountain unsaturated zone groundwaters could evolve through evaporation into brines characterized by very low deliquescence points, high chloride concentration, and low concentrations of anions such as nitrate and sulfate that could mitigate against the chloride-enhanced corrosion of the waste package. Qualitative information derived from a chemical divide approach, however, suggests that only approximately 8 percent of the reported unsaturated zone groundwater composition would evolve into that type of brine. The other 92 percent of the groundwater compositions

considered in the analysis would form brines that have lower deliquescence points than pure $NaNO_3$, but not as low as the other type. Thermodynamic simulations also show that if fluoride ions are present in the groundwater, evaporative concentration would lead to fluoride concentrations that are above the threshold for accelerated corrosion of the titanium drip shield.

The results of relative conductivity measurements indicate that as the relative humidity increases, the conductivity of a dry salt or salt mixture starts to increase at a humidity value significantly lower than the deliquescence point of the salt or salt mixture. This increase in conductivity implies initiation of drip shield or waste package aqueous corrosion may occur at a relative humidity significantly lower than the deliquescence point of the salt mixture deposited on them. Corrosion behavior under such environments needs to be considered in performance assessment.

TABLE OF CONTENTS

FIGURES

TABLES

ACKNOWLEDGMENTS

This report was prepared to document work performed by the Center for Nuclear Waste Regulatory Analyses (CNWRA) for the U.S. Nuclear Regulatory Commission (NRC) under Contract No. NRC–02–97–009. The activities reported here were performed on behalf of the NRC Office of Nuclear Material Safety and Safeguards, Division of Waste Management. This report is an independent product of the CNWRA and does not necessarily reflect the views or regulatory position of the NRC.

QUALITY OF DATA, ANALYSES, AND CODE DEVELOPMENT

DATA: CNWRA-generated original data contained in this report meet quality assurance requirements described in the CNWRA Quality Assurance Manual. Sources for other data should be consulted for determining the level of quality for those data.

ANALYSES AND CODES: The computer software Environmental Simulation Program Version 6 and SOLCALC Version 1.0 were used in the analyses contained in this report. Environmental Simulation Program Version 6 is commercial software and only object codes are available to the CNWRA. SOLCALC Version 1.0 is an acquired software that was developed at the University of California, Berkeley, by the senior author (R. Pabalan). Its source code is available and may be modified at the CNWRA. Environmental Simulation Program Version 6 and SOLCALC Version 1.0 are presently under CNWRA configuration control as required by the Technical Operating Procedure (TOP)-018, Development and Control of Scientific and Engineering Software. A record of experimental and computational work is available in Scientific Notebook number 018E, 430, and 464.

1 INTRODUCTION

A key attribute of the U.S. Department of Energy (DOE) safety strategy for its proposed high-level waste repository at Yucca Mountain, Nevada, is the long life of waste packages and drip shields. The waste packages will consist of an outer container of a highly corrosion-resistant Ni-Cr-Mo alloy (Alloy 22) over an inner container made of Type 316 nuclear grade stainless steel. Extending over the length of the emplacement drifts and covering the waste packages will be an arched drip shield made of a Ti-Pd alloy (Ti Grade 7). Aside from failures by potential mechanical disruption, aqueous corrosion is expected to be the primary degradation process limiting the life of the waste package and drip shield (CRWMS M&O, 2000a). The type, the rate, and the duration of drip shield and waste package corrosion that may occur in a repository setting are dependent on water chemistry and temperature. For example, the general corrosion rate for Ti Grade 7 drip shields may be accelerated significantly by fluoride ions at concentrations as low as ~0.0005 M (Brossia and Cragnolino, 2001). High chloride concentrations can initiate localized corrosion of the Alloy 22 outer waste package materials, although other ions such as nitrate and sulfate may mitigate this effect to varying degrees (Cragnolino, et al., 2001).

Coupled thermal-hydrological-chemical processes could significantly alter the chemistry of groundwater that percolates through the rock, seeps into the repository drift, and contacts the waste package and drip shield. The chemical composition of seepage waters could evolve by interactions with condensed water and engineered structural materials. Water present in a hot repository setting will be subjected to evaporation processes that could increase the concentrations of chloride, fluoride, and other ions and lead to the accumulation of multicomponent salt deposits on drip shield and waste package surfaces. Additional salts, such as soluble chlorides, nitrates, and sulfates of sodium, potassium, calcium, and magnesium, that are present as aerosols in atmospheric air (Ge, et al., 1998) and entrained in ventilation air introduced into the repository drift also may be deposited on the drip shield and waste package surfaces (Bechtel SAIC Company, LLC, 2001). Inorganic salts are generally hygroscopic and will absorb moisture from humid air, generating small volumes of potentially corrosive brines. A phase change from a solid particle to a saturated aqueous phase usually occurs spontaneously when the relative humidity in the surrounding atmosphere increases to a level known as the deliquescence point or deliquescence relative humidity (Tang and Munkelwitz, 1993) (See Section 2).

In the DOE analysis of the engineered barrier subsystem chemical environment, it was assumed that sodium and potassium will be the major cations in concentrated Yucca Mountain waters, with sodium ions generally in excess of potassium ions (CRWMS M&O, 2000a). Therefore, it was considered by DOE that the hygroscopic salts that could deposit on the drip shield and waste package surfaces would be limited to either sodium or potassium salts, and that sodium nitrate ($NaNO_3$) will determine the minimum relative humidity at which aqueous films will form on the drip shield and waste package surface. The deliquescence relative humidity of $NaNO_3$ varies from 50 percent at the boiling point {121 °C [250 °F]} of the saturated solution to 73 percent at 30 °C [86 °F] (Bechtel SAIC Company, LLC, 2001). The DOE total system performance assessment model assumed that aqueous corrosion of waste package and drip shield begins when the relative humidity reaches the deliquescence relative humidity of pure $NaNO_3$ salt in the temperature range predicted for the geologic repository system (CRWMS M&O, 2000a,d). This assumption was considered conservative by DOE because

$NaNO_3$ has the lowest deliquescence relative humidity among the sodium and potassium salts expected by DOE to form in a repository environment (Figure 1-1). DOE also reported that deliquescence occurs at greater humidity for mixtures of salts than for single salts (DOE, 2000, p. 4–166). Literature data indicate the deliquescence relative humidity of mixed salts is always lower than the deliquescence relative humidity of individual salts (Wexler and Seinfeld, 1991; Yang, et al., 2001), and significant adsorption of water by the salt particle can occur at relative humidities lower than the deliquescence relative humidity (Ge, et al., 1998; Yang, et al., 2001). In addition, the DOE analysis did not consider the potential formation of magnesium or calcium salts, which have much lower deliquescence relative humidity than sodium or potassium salts. Relative humidity will increase as the repository cools, and a lower deliquescence relative

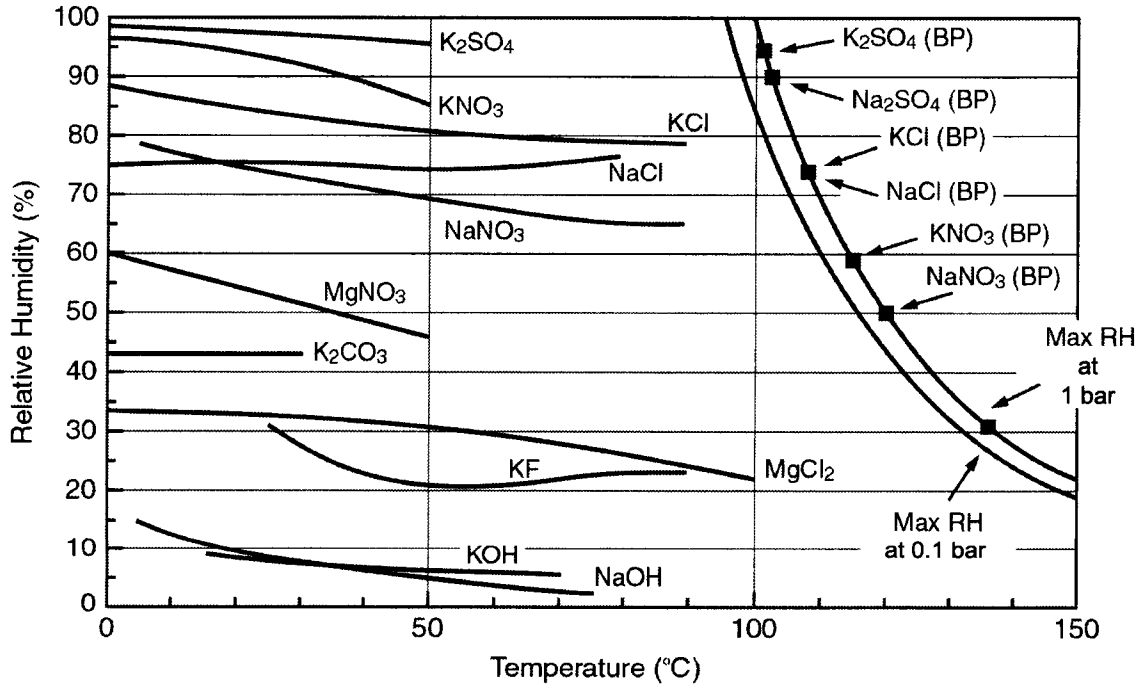

Figure 1-1. Handbook Data on Equilibrium Relative Humidity as a Function of Temperature for Saturated Solutions of Some Pure Salts. Each Curve Probably Terminates at the Boiling Curves to the Right, but There Are Gaps in the Available Handbook Data at Intermediate Temperature. Figure Modified from DOE (2000).

humidity means an earlier formation of a potentially corrosive brine. Thus, the $NaNO_3$ deliquescence relative humidity may not provide a realistic threshold for initiation of aqueous corrosion of waste package and drip shield surfaces. Because long-lived waste packages and drip shields are key attributes of the DOE safety strategy, staffs of the Center for Nuclear Waste Regulatory Analyses (CNWRA) and the U.S. Nuclear Regulatory Commission (NRC) are coordinating their efforts in the Evolution of the Near-Field Environment and the Container Life and Source Term Key Technical Issues to better understand the coupled thermal-hydrological-chemical processes and in-drift environmental conditions that may affect waste package and drip shield performance. This report describes the results of modeling and experimental studies pertaining to the plausible range of chemical conditions that may occur on the drip shield and waste package surfaces. Thermodynamic modeling was conducted to evaluate the effect of salt formation on the chemical environment of drip shields and waste packages at the proposed Yucca Mountain repository. The deliquescence behavior of salt mixtures was evaluated using thermodynamic considerations and compared with that of single salts. The chemical evolution of Yucca Mountain groundwaters was evaluated to determine the types of brines and salt mixtures that could form by evaporation processes. Implications of the deliquescence behavior of salt mixtures and the evaporation of Yucca Mountain groundwaters to the chemical environment on waste package and drip shield surfaces are discussed in this report.

To support the thermodynamic calculations, experimental determinations of the deliquescence points of electrolyte mixtures also were performed. The deliquescence relative humidities of salt mixtures containing sodium, potassium, nitrate, and chloride ions were measured because these data are not available from the literature. In addition, the relative values of ionic conductivity of various salts were measured because aqueous corrosion requires the presence of an electrolyte conductive to ionic species. The conductivity measurements were performed as a function of relative humidity at constant temperature. The minimum relative humidity at which conductivity starts to rise was compared to the deliquescence relative humidity of the salt.

2 THE CONCEPT OF DELIQUESCENCE RELATIVE HUMIDITY

The relative humidity, *RH*, is given by the equation

$$RH = pH_2O / pH_2O^{\circ} \qquad (2\text{-}1)$$

where pH_2O is the vapor pressure of an aqueous solution, and pH_2O° is the vapor pressure of pure water at the system temperature. At equilibrium, the liquid phase activity of water, a_w, is equal to RH.

As noted in the previous section, a solid salt particle transforms into a saturated aqueous solution when the relative humidity in the environment reaches the salt's deliquescence relative humidity. For single salts, the deliquescence relative humidity is characteristic of the particular salt and depends only on temperature (Wexler and Seinfeld, 1991). For mixtures of two or more salts, the deliquescence behavior is more complicated because their deliquescence relative humidities are a function of the mixture composition in addition to temperature. The minimum relative humidity at which the multicomponent salt mixture can deliquesce is known as mutual deliquescence relative humidity (Ge, et al., 1998). It is also known as the eutonic point (Tang and Munkelwitz, 1993). Below the mutual deliquescence relative humidity, a solid phase is thermodynamically favored. At the mutual deliquescence relative humidity, the aqueous phase is saturated with all of the salts. The mutual deliquescence relative humidity is the only relative humidity at which an aqueous solution can coexist with a precipitate composed of all the component salts (Pilinis, 1999).

The concept of relative humidity of deliquescence for salt mixtures is illustrated in Figure 2-1, which is a plot of the relative humidity at 25 °C [77 °F] over an aqueous solution saturated with either NaCl or $NaNO_3$, or both (Ge, et al., 1998). Consider, for instance, a solution of composition A. As the ambient relative humidity is lowered from RH_1 to RH_2, the solution eventually becomes saturated and precipitates $NaNO_3$ salt. As the ambient relative humidity is lowered further, more of the $NaNO_3$ crystallizes and the composition of the residual liquid evolves along the curve B-B_1, becoming more saturated with NaCl, until the mutual deliquescence relative humidity is reached. At the mutual deliquescence relative humidity, NaCl and $NaNO_3$ crystallize together and an aqueous phase with the eutonic composition B_1 is in equilibrium with both solids.

For bulk composition A, if the ambient relative humidity initially below the mutual deliquescence relative humidity is increased, no significant uptake of water by the NaCl+$NaNO_3$ salt mixture occurs until the mutual deliquescence relative humidity is reached. At the mutual deliquescence relative humidity, deliquescence occurs and the salt mixture dissolves—$NaNO_3$ partially and NaCl completely. As the ambient relative humidity is raised further, the amount of solid decreases and the amount of liquid increases, with the liquid becoming richer in dissolved $NaNO_3$ relative to dissolved NaCl. At a relative humidity slightly below RH_2, only a small amount of solid $NaNO_3$ remains and the composition of the liquid will have changed from B_1 to B. At RH_2, the $NaNO_3$ solid is completely dissolved and the liquid will have composition A.

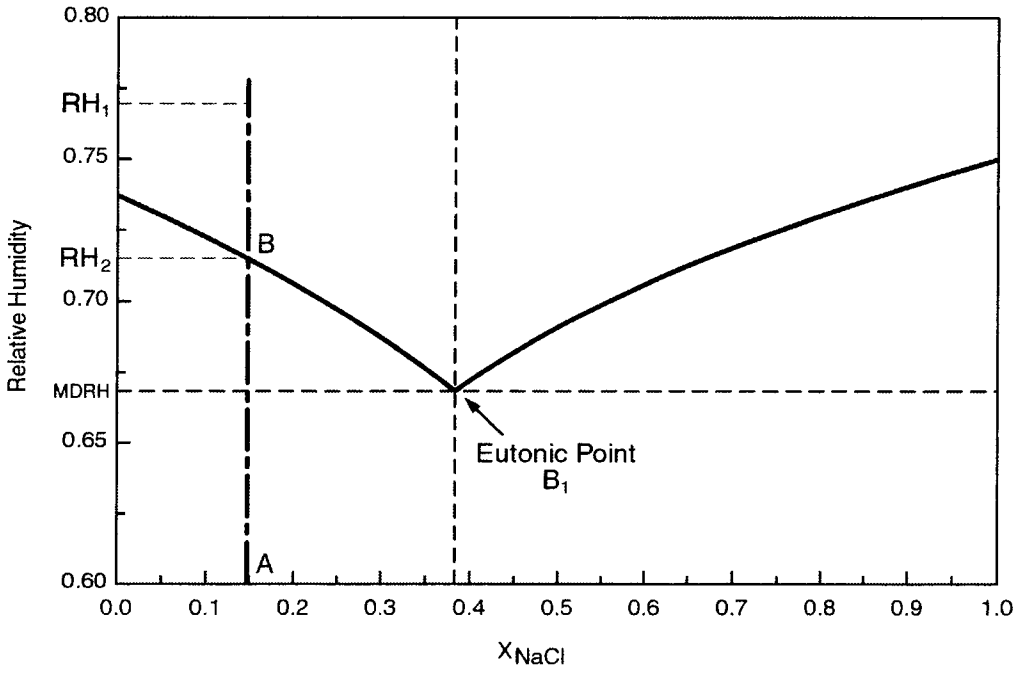

Figure 2-1. Relative Humidity (RH) over an Aqueous Solution of $NaNO_3$ and NaCl at 25 °C [77 °F] (Ge, et al., 1998). At X_{NaCl} to the Left of the Eutonic Composition B_1, the Solution Is Saturated with $NaNO_3$ Salt. At X_{NaCl} to the Right of B_1, the Solution Is Saturated with NaCl Salt. At B_1, the Solution Is Saturated with Both NaCl and $NaNO_3$ (MDRH = mutual deliquescence RH). Note that $X_{NaNO3} = 1 - X_{NaCl}$.

The mutual deliquescence relative humidity is always lower than the deliquescence relative humidity of the component salts (Wexler and Seinfeld, 1991). The system is said to be in a mutual deliquescence region when the ambient relative humidity is

$$\begin{aligned} &MDRH(\text{salt-1, salt-2,... salt-n}) \le RH \\ &< \min\left\{DRH_{\text{salt-1}}, DRH_{\text{salt-2,...}} DRH_{\text{salt-n}}\right\} \end{aligned} \tag{2-2}$$

Neglecting mutual deliquescence for salt mixtures ignores the interactions among the different ions present in the mixture and leads to the erroneous prediction of a dry salt mixture for cases where the relative humidity lies in a mutual deliquescence region (Pilinis, 1999). This neglect potentially can affect the predicted role of corrosive brines in the degradation of drip shield and waste package materials.

3 CALCULATION OF MUTUAL DELIQUESCENCE RELATIVE HUMIDITY

Experimental data on the deliquescence relative humidity of many single salts in the temperature range 0 to 100 °C [32 to 212 °F] are available in the literature (Greenspan, 1977). Data on the mutual deliquescence relative humidity of salt mixtures are sparse. Although substantial research has been reported in recent years on the deliquescence behavior of mixed salts as a function of ambient relative humidity and temperature (e.g., Ge, et al., 1998; Tang and Munkelwitz, 1993), these studies were done from the perspective of atmospheric chemistry, and the temperature range studied is much lower than that expected in a heated repository environment. Deliquescence humidities of multicomponent inorganic salt mixtures, however, can be predicted from the thermodynamic properties in the solid-liquid coexistence region (Tang and Munkelwitz, 1993). Thus, for this study, thermodynamic calculations were used to derive the mutual deliquescence relative humidity of salt mixtures.

The deliquescence relative humidity of a single salt or mutual deliquescence relative humidity of a salt mixture is the critical humidity at which the salt or salt mixture abruptly transforms from a crystalline state to a saturated aqueous phase. The deliquescence relative humidity and mutual deliquescence relative humidity also can be viewed as the equilibrium relative humidity above an aqueous solution that is saturated with respect to the solid(s) it contains. Thus, the dissolved concentration at the deliquescence point is the same as the solubility of the salt(s) at that temperature.

The thermodynamic approach used here is based on calculating the osmotic coefficient, ϕ, of an aqueous solution that is saturated with a salt or salt mixture of interest. The calculation requires data on (i) the standard-state chemical potential of solids and aqueous species at the temperature and pressure of interest and (ii) the activity coefficient of aqueous species as functions of solution composition, temperature, and pressure. The equations and parameter values used to derive (i) and (ii) are given by Pabalan and Pitzer (1987, 1991), who calculated salt solubilities, as well as vapor pressure depression and boiling point elevation (Pabalan and Pitzer, 1990), of multicomponent salt mixtures in the system Na-K-Mg-Cl-SO_4-OH-H_2O using the Pitzer model for aqueous activity coefficients (Pitzer, 1973; 1991).

Once the osmotic coefficient of a solution saturated with a salt or salt mixture is calculated, the activity of water in the saturated solution can be derived from the following equation relating water activity to osmotic coefficient (Pabalan and Pitzer, 1987)

$$\ln a_w = -\phi \left(M_w / 1{,}000 \right) \sum_i m_i \qquad (3\text{-}1)$$

where M_w is the molecular mass of water, m_i is the molality (moles/kg H_2O) of species i, and the summation covers all solute species. Deliquescence relative humidity or mutual deliquescence relative humidity is simply equal to a_w of the saturated solution.

The mutual deliquescence relative humidity for two- and three-salt mixtures in the system NaCl-KCl-$MgCl_2$ was calculated using Eqs. (2-1) and (3-1) together with the equations and parameters given in Pabalan and Pitzer (1987, 1991), and the program SOLCALC (Pabalan, 2002), Sodium, potassium, magnesium, and calcium are the dominant cations in Yucca Mountain groundwaters, whereas chloride is a dominant anion along with bicarbonate or

carbonate, sulfate, and nitrate (Yang, et al., 1996, 1998). The calculations were made using a temperature of 90 °C [194 °F], a minimum value that can be sustained at the waste package and drip shield surfaces for more than 1,000 years in a repository in a high-temperature operating mode (Painter, et al., 2001). Note that, in general, the mutual deliquescence relative humidity for a given salt mixture composition decreases with increasing temperature (Tang and Munkelwitz, 1993).

The calculated mutual deliquescence relative humidities for the two-salt mixtures NaCl+KCl, NaCl+$MgCl_2$, and KCl+$MgCl_2$ at 90 °C [194 °F] are shown in Figure 3-1. For comparison, the reported 90 °C [194 °F] deliquescence relative humidity for a pure $NaNO_3$ salt (Greenspan, 1977) also is plotted. In each case, the mutual deliquescence relative humidity for the salt mixture is lower than the deliquescence relative humidity of the individual salts. For the mixture of NaCl and KCl, both of which have relatively high deliquescence relative humidity, the depression of deliquescence point caused by the other salt is not large—less than 10-percent deliquescence relative humidity, and the mutual deliquescence relative humidity of NaCl+KCl is always higher than the deliquescence relative humidity of a pure $NaNO_3$ salt at the same temperature. In contrast, the deliquescence point of NaCl or KCl is substantially reduced when mixed with $MgCl_2$, which has a 90 °C [194 °F] deliquescence relative humidity equal to 25 percent, and can be much lower than that of pure $NaNO_3$ salt. The significant reduction in mutual deliquescence relative humidity for $MgCl_2$ is further illustrated in Figure 3-2, a plot of the mutual deliquescence relative humidity for mixtures of the three salts NaCl, KCl, and $MgCl_2$. In the ternary mixture, the lowest mutual deliquescence relative humidity is calculated to be 24.2 percent for a solution saturated with the solids halite+carnallite+bischofite.

A lower deliquescence point potentially could lead to earlier and hotter initiation of aqueous corrosion of the waste package and drip shield. Furthermore, the chloride concentration of brine solutions containing $MgCl_2$ can be extremely high–up to ~15 m (stoichiometric value), which can be deleterious to the performance of the waste package material.

A similar lowering in deliquescence point and increase in chloride concentration are expected for mixtures with $CaCl_2$, another salt with high solubility and very low deliquescence relative humidity (Cohen, et al., 1987a). The nitrate salts of magnesium and calcium also have much lower deliquescence points than the chloride and nitrate salts of potassium and sodium (Greenspan, 1977). Furthermore, the solubility of magnesium and calcium nitrates are much higher than those of magnesium and calcium chlorides. For example, at 90 °C [194 °F], the solubility of $MgCl_2$ is 7.2, of $Mg(NO_3)_2$ is 16.2, of $CaCl_2$ is 13.0, and of $Ca(NO_3)_2$ is 22.0 (Lide, 2001). Thus, the potential formation of salt mixtures with magnesium and calcium is important to consider in evaluating the chemical environment on the surface of the waste package and drip shield.

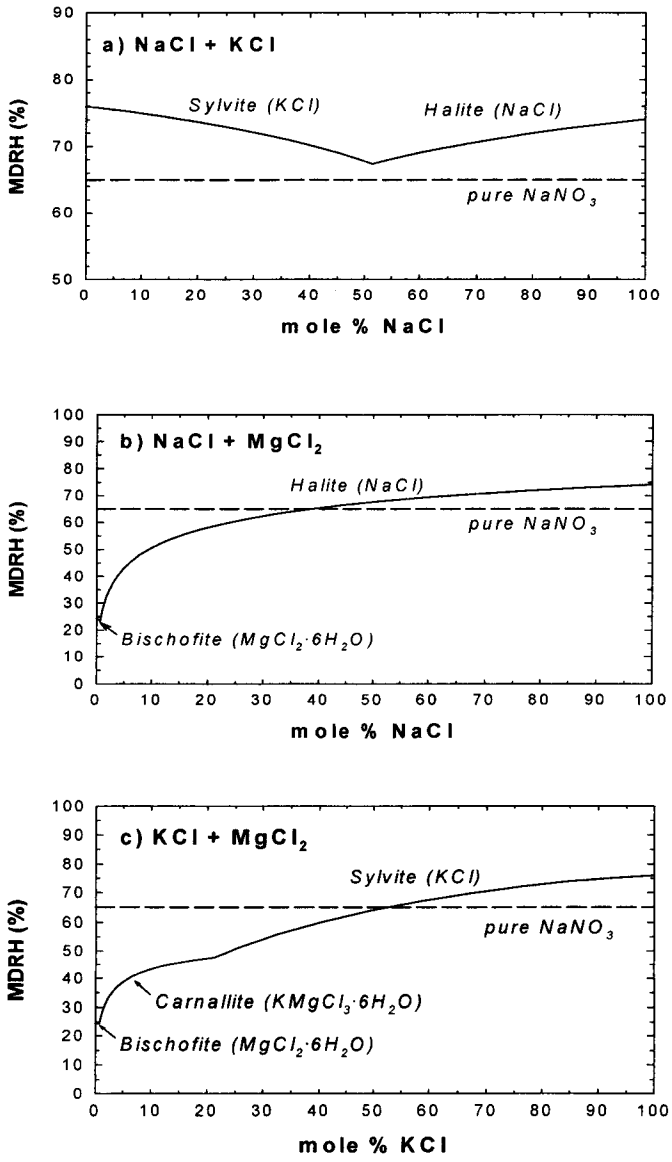

Figure 3-1. Calculated Mutual Deliquescence Relative Humidity (MDRH) (%), at 90 °C [194 °F] for Mixtures of (a) NaCl+KCl, (b) NaCl+$MgCl_2$, and (c) KCl+$MgCl_2$. The Solutions Are Saturated with the Indicated Solids. The Deliquescence Relative Humidity of a Pure $NaNO_3$ Salt at 90 °C [194 °F] Reported in Greenspan (1977) Also Is Shown for Comparison (Dashed Line).

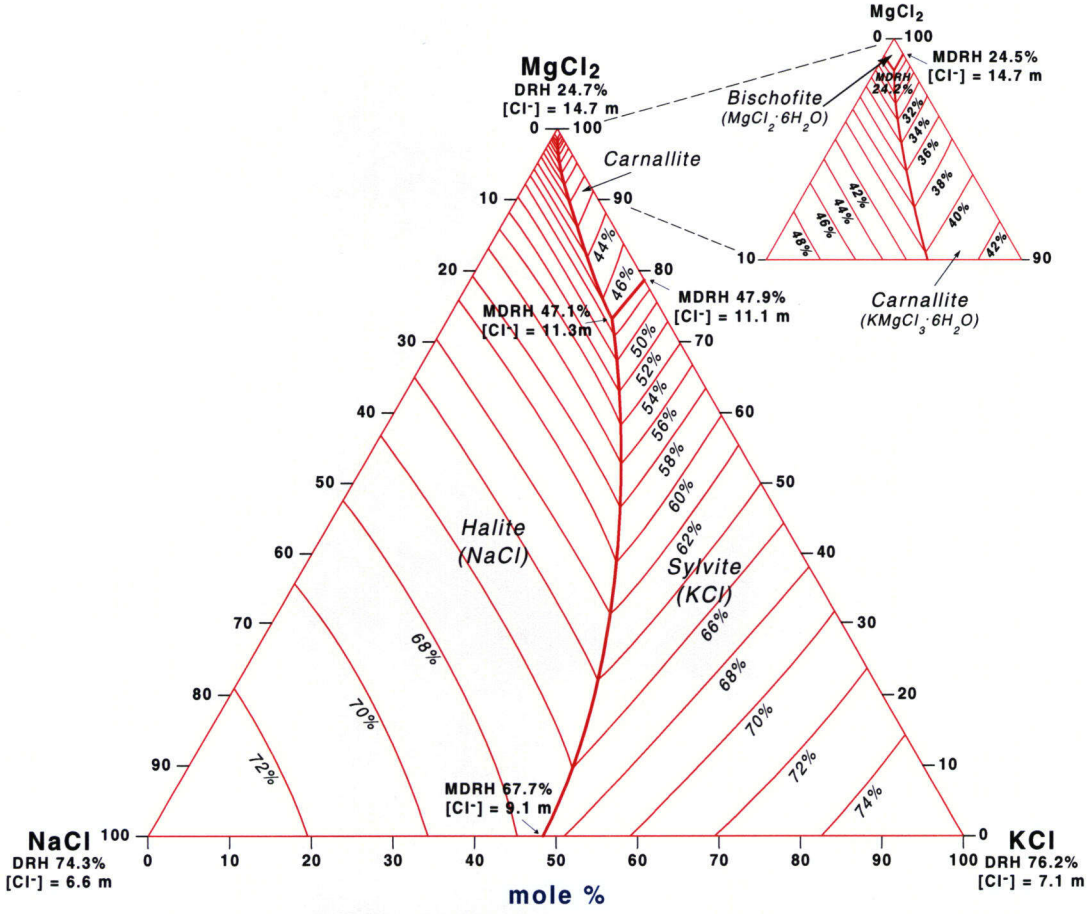

Figure 3-2. Calculated Mutual Deliquescence Relative Humidity (MDRH) (%), Shown as Contour Lines, of Salt Mixtures in the System NaCl-KCl-$MgCl_2$ at 90 °C [194 °F]. The Solutions Are Saturated with the Indicated Solids. Also Shown for Some Compositions Is the Calculated Stoichiometric Chloride Concentration, [Cl^-] (moles/kg H_2O), of the Saturated Solution.

4 EVOLUTION OF YUCCA MOUNTAIN GROUNDWATER CHEMISTRY

The chemical evolution of Yucca Mountain groundwaters was evaluated to determine the types of brines and salt mixtures that could form by evaporation processes. Two methods were used: (i) thermodynamic simulation using a computer program and (ii) analysis based on the concept of chemical divides.

4.1 Thermodynamic Simulation

Thermodynamic calculations were conducted using the Environmental Simulation Program Version 6. Environmental Simulation Program Version 6 is a steady-state process simulator developed by OLI Systems, Inc. (Morris Plains, New Jersey) for evaluating aqueous chemical processes in industrial and environmental applications. Environmental Simulation Program Verison 6 was used in this study because it is valid to much higher solution concentrations than geochemical codes, such as EQ3/6 (Wolery, 1992), and has a larger database of thermodynamic parameters. Environmental Simulation Program Version 6 represents standard-state properties using the Helgeson-Kirkham-Flowers (Helgeson, et al., 1981) equation-of-state and excess properties using the aqueous activity coefficient expressions developed by Bromley (1972) and Pitzer (1973, 1991). These models enable simulation of aqueous chemical systems using Environmental Simulation Program Version 6 for temperatures to 300 °C [572 °F], pressures to 1,500 bar [1,400 atm], and ionic strengths as high as 30 molal. The ionic strength limit restricts evaporation simulation to one mole fraction of water in solution of approximately 0.65, and the chemical evolution of the water chemistry cannot be followed to complete evaporation. Nevertheless, the concentration limit is high enough to allow the general trends in chemical evolution of Yucca Mountain groundwaters to be identified. Ongoing development work by OLI Systems, Inc. is expected to extend the capability of Environmental Simulation Program Version 6 to permit simulation to complete evaporation.

The unsaturated zone at Yucca Mountain contains pore water, fracture water, and isolated lenses of perched water. Yang, et al. (1996, 1998) measured chemical compositions of pore water and perched water from Yucca Mountain. Perched waters were sampled from boreholes using plastic bailers, and pore waters were extracted from borehole core samples using high-pressure uniaxial compression techniques. Although there are significant uncertainties in the pore water chemistry data resulting from the air drilling of core samples, pore water evaporation, and the compression techniques (Browning, et al., 2000; Yang, et al., 1996, 1998), they provide a valuable characterization of groundwater chemistry at Yucca Mountain. No measured compositions of Yucca Mountain fracture waters are available because these waters are difficult to sample. Samples of fracture water, however, have been collected at Rainier Mesa, located approximately 50 km [31 mi] north-northeast of Yucca Mountain, and those samples are similar in composition to perched and saturated zone waters collected at Yucca Mountain. The saturated zone groundwaters lie below the proposed repository site, and samples of this water, pumped from the J–13 Well water, have been used extensively by DOE as a reference Yucca Mountain groundwater composition for experimental studies (CRWMS M&O, 1998; Rosenberg, et al., 1999).

The analysis presented in this section assumes that water entering the repository drift will have characteristics similar to those sampled at Yucca Mountain under ambient conditions. Changes in the composition of seepage waters through their interaction at elevated temperature with the

rocks or with engineered materials, such as rock bolts and grout, are neglected. For the analysis, several Yucca Mountain pore water compositions were selected from the compilation of Yang, et al. (1996, 1998) to represent a relatively broad range of ambient system water chemistry and were used as input to the evaporation simulations. J–13 Well water composition, reported as averaged values by Harrar, et al. (1990), was used also because it is similar to the composition of perched waters and because experimental and modeling results on J–13 Well water evaporation have been reported by DOE (Rosenberg, et al., 1999). The selected water compositions are listed in Table 4-1 and plotted as Piper diagrams in Figure 4-1(a). Note that only J–13 Well water has reported potassium and fluoride ion concentrations.

Evaporation was simulated at different temperatures but at a constant atmospheric pressure of 0.85 bar, which is the approximate atmospheric pressure at Yucca Mountain. The results at 110 °C [230 °F] are shown in Table 4-2 and Figure 4-1(b). The results indicate that of the seven compositions selected, four (J–13 Well water, UZ–14/85.2–85.6, UZ–14/1,542.3–1,542.8, NRG–6/244.6–245.0) evolved toward a (Na±K)-(Cl±NO_3) type of brine. Complete evaporation of this brine likely would form a salt mixture with a mutual deliquescence relative humidity that is lower relative to pure $NaNO_3$ salt. For example, the mutual deliquescence relative humidity for a NaCl+$NaNO_3$+KNO_3 mixture measured at 86 °C [187 °F] is 43 percent, compared to a measured value of 65 percent for pure $NaNO_3$ (Yang, et al., 2001). Evaporation of water with compositions similar to the other three Yucca Mountain groundwater samples, UZ–14/1,277.7–1,278, NRG–6/158.2-158.6, and SD–9/94.2–94.4, led to formation of a (Mg+Ca+Na)-Cl brine. Complete evaporation of this brine type would lead to salt mixtures with an even lower mutual deliquescence relative humidity because of the presence of magnesium and calcium chlorides.

The brines resulting from evaporation of Yucca Mountain groundwaters all have elevated concentrations of chloride ions, which could make the waste package materials possibly more susceptible to localized corrosion. The evaporated UZ–14/1,277.7–1,278, NRG–6/158.2–158.6, and SD–9/94.2–94.4 waters have the highest chloride concentrations (as high as 10 m free Cl^- ion), but also have very low nitrate and sulfate concentrations (less than 0.01 and 0.0001 m). In these solutions, sulfate ion concentration is constrained by precipitation of calcium and magnesium sulfates, whereas nitrate ion concentration is kept low by the formation of aqueous calcium nitrate complexes. The observed very low concentrations of nitrate and sulfate ions are important because at these concentrations, nitrate and sulfate likely would not inhibit localized corrosion of the waste package (Cragnolino, et al., 2001). The evolved J–13 Well water, UZ–14/85.2–85.6, UZ–14/1,542.3–1,542.8, NRG–6/244.6–245.0 all have very high nitrate concentrations (as high as 9 m), thus the potential for inhibition of localized corrosion in these waters is much greater.

An important factor to consider with respect to the corrosion of the titanium drip shield is the effect of fluoride ion. Potentiostatic measurements of the polarization behavior of Ti Grade 7 in deaerated 1-M NaCl solutions at 95 °C [203 °F] indicated that accelerated general corrosion of the titanium alloy occurs when fluoride ions are present at a concentration ~0.0005 M or greater (Brossia and Cragnolino, 2001). This threshold fluoride concentration can be achieved by evaporation of groundwater. For example, the Environmental Simulation Program Version 6 simulation shows that a fluoride concentration equal to 0.14 m can result from evaporation of J–13 Well water at 110 °C [230 °F] at a concentration factor of 15,000×. Other data (Brossia and Cragnolino, 2001) indicate that the deleterious effect of fluoride is not altered by the

Table 4-1. Compositions (moles/liter) of Yucca Mountain Unsaturated Zone Pore Water Samples from Boreholes USW UZ–14, NRG–6, and SD–9, Reported by Yang, et al. (1996, 1998) and Average J–13 Well Water Composition Reported by Harrar, et al. (1990). The Identification for the UZ–14, NRG–6, and SD–9 Samples Gives the Sampling Depth (in feet).

Species	UZ–14/ 85.2–85.6	UZ–14/ 1,277.7–1278	UZ–14/ 1,542.3–1,542.8	NRG–6/ 158.2–158.6	NRG–6/ 244.6–245.0	SD-9/ 94.2–94.4	Average J–13 Well Water
Ca^{2+}	1.25×10^{-3}	1.85×10^{-3}	8.98×10^{-5}	3.04×10^{-3}	8.23×10^{-4}	3.12×10^{-3}	3.24×10^{-4}
Mg^{2+}	5.43×10^{-4}	2.10×10^{-4}	2.06×10^{-5}	9.59×10^{-4}	2.02×10^{-4}	9.87×10^{-4}	8.27×10^{-5}
Na^{+}	1.89×10^{-3}	1.96×10^{-3}	9.00×10^{-3}	1.55×10^{-3}	3.13×10^{-3}	1.87×10^{-3}	1.99×10^{-3}
K^{+}	N/A	N/A	N/A	N/A	N/A	N/A	1.29×10^{-4}
$SiO_2(aq)$	1.49×10^{-3}	6.32×10^{-4}	2.38×10^{-3}	1.62×10^{-3}	8.49×10^{-4}	1.23×10^{-3}	1.02×10^{-3}
Al^{3+}	1.11×10^{-5}	N/A	5.11×10^{-4}	0	2.22×10^{-5}	N/A	0
HCO_3^{-}	2.15×10^{-3}	2.79×10^{-3}	6.29×10^{-3}	5.57×10^{-4}	1.00×10^{-3}	6.06×10^{-4}	2.11×10^{-3}
CO_3^{2-}	0	0	7.67×10^{-4}	0	0	0	0
Cl^{-}	1.69×10^{-3}	3.67×10^{-3}	5.64×10^{-4}	5.22×10^{-3}	1.38×10^{-3}	4.80×10^{-3}	2.01×10^{-4}
NO_3^{-}	3.55×10^{-4}	2.42×10^{-4}	6.45×10^{-5}	5.16×10^{-4}	6.45×10^{-4}	1.77×10^{-4}	1.42×10^{-4}
SO_4^{-}	6.87×10^{-4}	3.96×10^{-4}	2.91×10^{-4}	1.66×10^{-3}	1.20×10^{-3}	2.71×10^{-3}	1.92×10^{-4}
F^{-}	N/A	N/A	N/A	N/A	N/A	N/A	1.15×10^{-4}
pH	6.9	N/A	8.6	6.8	7.2	6.2	7.41

Yang, I.C., G.W. Rattray, and Y. Pei. "Interpretation of Chemical and Isotopic Data from Boreholes in the Unsaturated Zone at Yucca Mountain, Nevada." Water-Resources Investigations Report 96-4058. Denver, Colorado: U.S. Geological Survey. 1996.

Yang, I.C., P. Yu, G.W. Rattray, J.S. Ferarese, and J.N. Ryan. "Hydrochemical Investigations in Characterizing the Unsaturated Zone at Yucca Mountain, Nevada." Water-Resources Investigations Report 98-4132. Denver, Colorado: U.S. Geological Survey. 1998.

Harrar, J.E., J.F. Carley, W.F. Isherwood, and E. Raber. "Report of the Committee to Review the Use of J–13 Well Water in Nevada Nuclear Waste Storage Investigations." UCID–21867. Livermore, California: Lawrence Livermore National Laboratory. 1990.

presence of either nitrate or sulfate ions. Thus, the importance of fluoride ions in affecting the long-term performance of the titanium drip shield cannot be neglected.

4.2 Chemical Divide Approach

The thermodynamic simulation of Yucca Mountain groundwater evaporation presented in the preceding section used only a small set of the groundwater chemistry data presented by Yang, et al. (1996, 1998) because simulations are time-intensive. To consider the full set of the Yang, et., data, an alternative approach based on the concept of chemical divides developed by

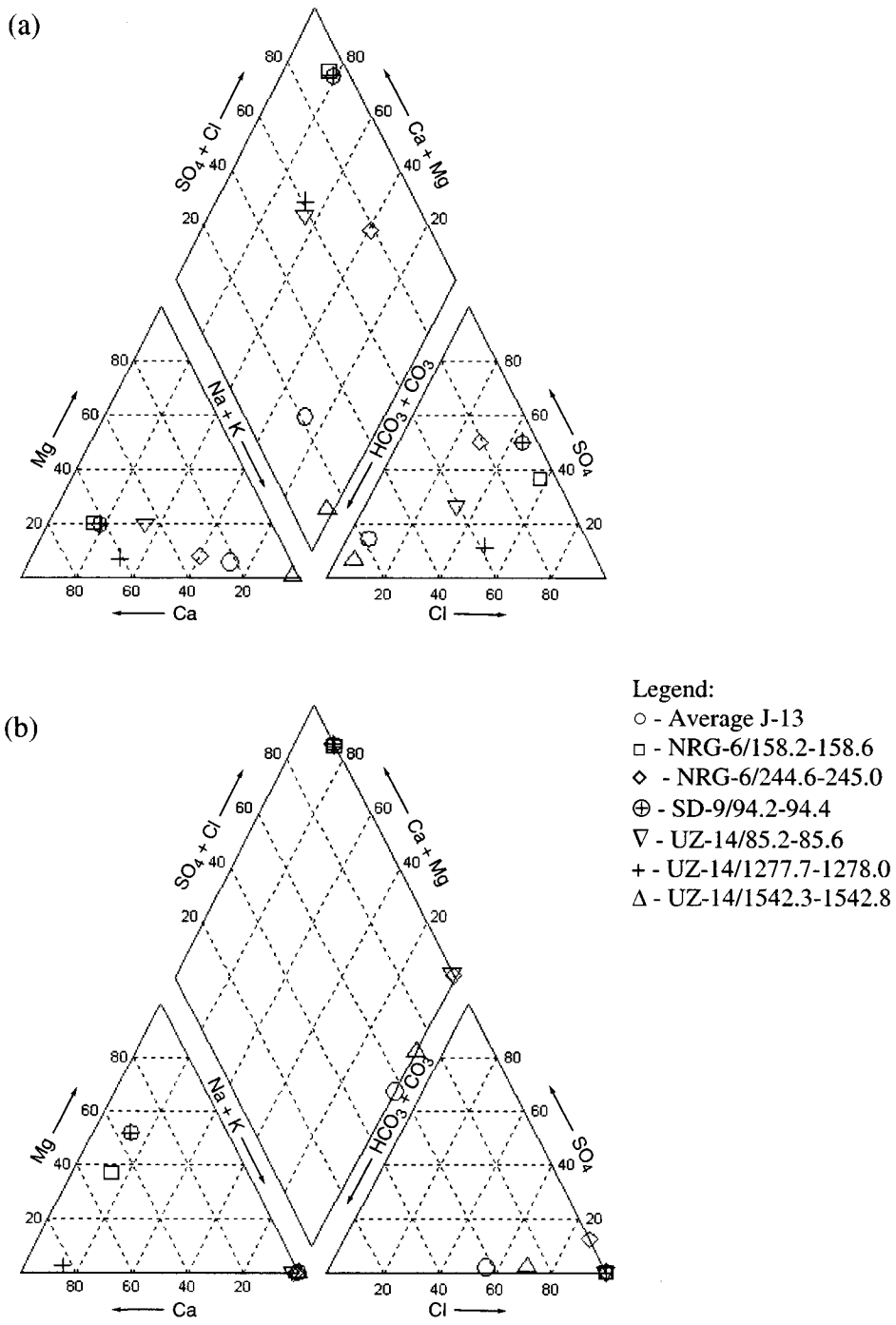

Figure 4-1. Compositions of Yucca Mountain Groundwaters (a) Before (see Table 4-1) and (b) After (see Table 4-2) Evaporation at 100 °C [212 °F] and 0.85 bar [0.84 atm]. Units in Percentage of Milliequivalents Per Liter.

Hardie and Eugster (1970) was used. The chemical divide concept is based on the early precipitation of relatively insoluble minerals, such as calcite and gypsum, and is used to determine the chemical type of brines and the salt minerals that form because of evaporative concentration of natural waters.

The concept of chemical divides is illustrated in Figure 4-2, which is a ternary phase diagram for the system Ca^{2+}-SO_4^{2-}-HCO_3^-. The composition of calcite ($CaCO_3$) plots at the midpoint of the Ca^{2+}-HCO_3^- join, whereas that of gypsum at the midpoint of the Ca^{2+}-SO_4^{2-} join.

The solubility of calcite is much less than that of gypsum. Thus, the primary stability field of calcite covers most of the diagram, and the primary stability field for gypsum is restricted to a narrow band along the Ca^{2+}-SO_4^{2-} join (Spencer, 2000). The primary stability field determines which mineral precipitates first from a solution of a specific water composition. For example, calcite is the first mineral to precipitate from waters whose composition falls within the bulk of this compositional triangle.

Subsequent to precipitation of a mineral, the solution composition moves directly away from the composition of that mineral on the diagram. Two chemical divides, one along the Ca^{2+}-SO_4^{2-} join and the other along the calcite-gypsum join, separate the Ca^{2+}-SO_4^{2-}-HCO_3^- diagram into three fields corresponding to three distinct water types: (i) alkaline, (ii) calcium-chloride, and (iii) neutral waters or brines. Alkaline waters, with mole-equivalents of HCO_3^- greater than that of Ca^{2+}, fall within the Ca^{2+}-SO_4^{2-}-HCO_3^- subtriangle. On evaporation, alkaline waters precipitate calcite, and their compositions evolve toward the SO_4^{2-}-HCO_3^- join, resulting in brines that are calcium-free (or have very low Ca^{2+} concentrations) and enriched in SO_4^{2-} and HCO_3^-. The pH of these waters is high because of the elevated HCO_3^- concentration. Average river waters generally lie within the alkaline field.

Calcium-chloride waters, with mole-equivalents of Ca^{2+} greater than the combined mole-equivalents of SO_4^{2-} and HCO_3^-, fall within the Ca^{2+}-calcite-gypsum subtriangle. Precipitation of calcite moves the composition of these waters to the univariant curve dividing the primary stability fields for calcite and gypsum. After intersecting the univariant curve, these waters precipitate both calcite and gypsum, and the solution composition evolves toward the Ca^{2+} corner of the diagram. After the precipitation of calcite and gypsum, Ca-chloride brines are depleted in both SO_4^{2-} and HCO_3^-.

Neutral brines fall in the third subtriangle of the diagram. The mole-equivalents of Ca^{2+} in these brines are greater than that of HCO_3^- but less than the combined SO_4^{2-} and HCO_3^- mole-equivalents. As in the case of calcium-chloride brines, precipitation of calcite leads waters to the univariant curve dividing the primary stability fields for calcite and gypsum. Waters in the neutral field, however, move toward the SO_4^{2-} corner of the diagram as both calcite and gypsum precipitate. After the precipitation of calcite and gypsum, neutral brines are depleted in both Ca^{2+} and HCO_3^-. Modern seawater falls within the neutral field.

Figure 4-3 is a ternary plot of the compositions of the seven Yucca Mountain groundwaters selected previously for thermodynamic simulations. These compositions were plotted also in a Piper diagram shown in Figure 4-1(a). Figure 4-3 shows that, of the four Yucca Mountain groundwater samples calculated to evolve toward a (Na±K)-(Cl±NO_3) type of brine, two (UZ–14/85.2–85.6, NRG–6/244.6–245.0) plot in the neutral brine field and the other two (J–13 Well water, UZ–14/1,542.3–1,542.8) plot in the alkaline brine field. In general, the

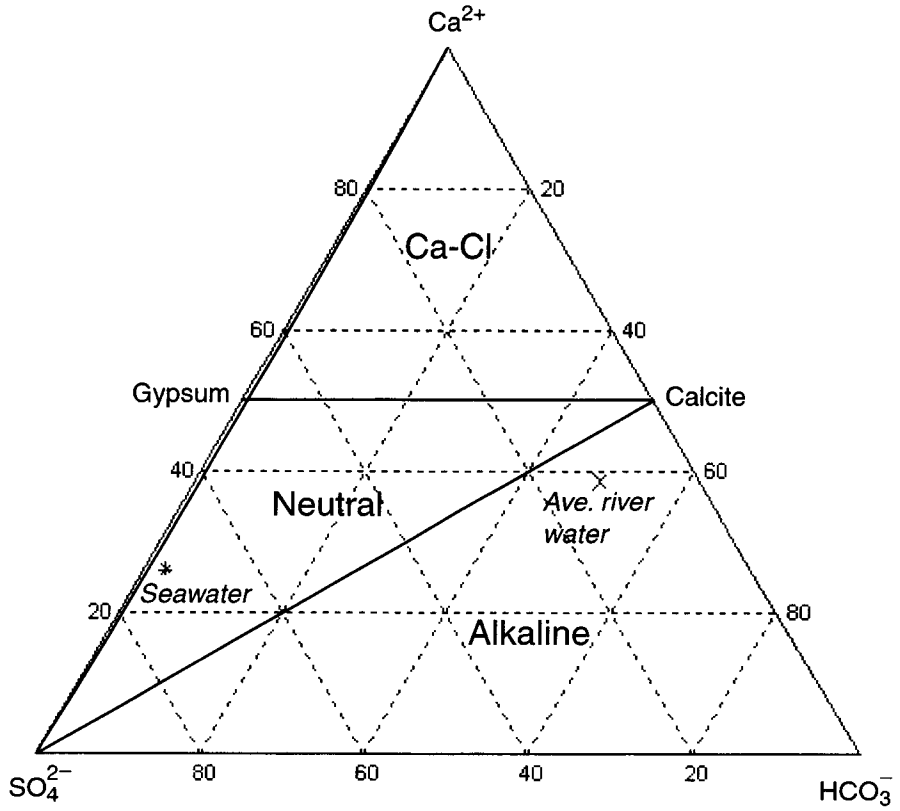

Figure 4-2. Ternary Phase Diagram for Ca^{2+}-SO_4^{2-}-HCO_3^- Illustrating the Concept of Chemical Divides. The Bulk of the Diagram is the Primary Stability Field of Calcite; the Gypsum Stability Field is Along the Ca^{2+}-SO_4^{2-} Join. Chemical Divides from Calcite to Sulfate and From Calcite To Gypsum Separate the Diagram Into Three types of Brines—Alkaline, Neutral, and Calcium-Chloride Type. Unit of Mole-Equivalent.

classification into neutral and alkaline brines based on the chemical divide approach is consistent with the results of thermodynamic calculations. For example, a comparison of initial and final concentrations given in Tables 4-1 and 4-2, respectively, shows that the J–13 Well water and UZ–14/1,542.3–1,542.8 both evolved into brines that are calcium-free, enriched in SO_4^{2-} and HCO_3^- (by a factor of approximately 300), and have alkaline pH (11.0 and 10.6). For the samples UZ-14/85.2-85.6 and NRG-6/244.6-245.0, values in Tables 4-1 and 4-2 show that both samples evolved into brines depleted in HCO_3^- with neutral pH (7.5 and 7.9). The final Ca^{2+} concentrations of UZ–14/85.2–85.6 and NRG-6/244.6-245.0, however, are higher by a factor of approximately 80 relative to the initial Ca^{2+} concentrations, which is inconsistent with the expected Ca^{2+} depletion based on the chemical divide approach.

The three Yucca Mountain groundwater compositions (UZ–14/1,277.7–1,278, NRG–6/158.2–158.6, and SD–9/94.2–94.4) calculated to evolve, upon evaporation, into (Mg+ Ca+Na)-Cl brines plotted in the calcium-chloride brine subtriangle of Figure 4-3. The location of these compositions in the ternary Ca^{2+}-SO_4^{2-}-HCO_3^- diagram is consistent with the results of thermodynamic calculations, which indicated that these waters evolve into brines comprised predominantly of calcium (plus magnesium) and chloride ions, with pH

approximately 6.0. Relative to the initial Ca^{2+} and Mg^{2+} concentrations (Table 4-1), the evolved compositions calculated for the UZ–14/1,277.7–1,278, NRG–6/158.2–158.6, and SD–9/94.2–94.4 samples are higher by three to four orders of magnitude.

The generally good agreement between the thermodynamic simulations and the chemical divide approach suggests that the latter could provide qualitative information on the chemistry of Yucca Mountain groundwaters that have undergone evaporative concentration. The compositions reported by Yang, et al. (1996, 1998) for 152 Yucca Mountain groundwater samples are plotted in a chemical divide diagram shown in Figure 4-4. Of the 152 samples, 12 plot in the calcium-chloride field, 27 plot in the neutral field, and 113 plot in the alkaline field. Thus, only approximately 8 percent of the Yucca Mountain water compositions reported by Yang, et al. (1996, 1998) are predicted to evolve into brines rich in either calcium or magnesium, or both. These brines, if evaporated completely, could form salt mixtures with very low deliquescence points. In contrast, 92 percent of the compositions reported by Yang, et al. (1996, 1998) are predicted to form (Na±K)-(Cl±NO_3) brines, mostly with alkaline pH. Complete evaporation of these brines would form salts that would have deliquescence points lower than pure $NaNO_3$, but the deliquescence points would not be as low as those of the calcium-magnesium types. This type of data may be used to develop probability distributions of deliquescence points for use in performance assessment.

Table 4-2. Calculated pH and Concentrations (molal) of Yucca Mountain Groundwaters After Evaporation at 110 °C [212 °F] and 0.85 bar [0.84 atm]. The Tabulated Values Are for Free (Uncomplexed) Ionic Species. Also Listed Are the Calculated Concentration Factor (Initial Water Mass/Final Water Mass) and Ionic Strength.

Ionic Species	UZ–14/ 85.2–85.6	UZ–14/ 1,277.7–1,278	UZ–14/ 1,542.3–1,542.8	NRG–6/ 158.2–158.6	NRG–6/ 244.6–245.0	SD–9/ 94.2–94.4	Average J–13 Well Water
Ca^{2+}	0.107	3.47	0	2.01	0.0601	1.44	0
Mg^{2+}	2.48×10^{-4}	0.0936	0	1.51	4.52×10^{5}	2.14	0
Na^{+}	10.4	1.21	11.1	1.15	12.7	1.12	7.67
K^{+}	not incl.	not incl.	not incl.	not incl.	not incl.	not incl.	1.88
$H_3SiO_4^{-}$	9.42×10^{9}	7.33×10^{6}	3.75×10^{7}	9.70×10^{10}	3.64×10^{8}	2.00×10^{6}	8.83×10^{-5}
$Al(OH)_4$	4.06×10^{10}	0	5.49×10^{9}	0	2.10×10^{9}	0	0
HCO_3^{-}	3.14×10^{9}	1.05×10^{7}	0.0124	0	3.34×10^{6}	9.07×10^{9}	0.0119
CO_3^{2-}	1.55×10^{10}	5.30×10^{10}	0.820	0	4.07×10^{-7}	1.65×10^{11}	1.13
Cl^{-}	4.79	10.0	4.17	9.33	3.85	8.76	2.95
NO_3^{-}	7.96×10^{3}	0.00917	4.52	0.00866	9.14	0.00547	2.08
SO_4^{2-}	4.98×10^{5}	7.48×10^{6}	0.0664	1.34×10^{5}	0.269	2.12×10^{5}	0.0521
F^{-}	not incl.	not incl.	not incl.	not incl.	not incl.	not incl.	0.135
Ionic strength	13.0	13.6	12.0	12.9	13.8	12.3	11.2
Conc. factor	29,000	7,036	1,000,000	2,200	15,000	2,771	15,000
pH	7.5	6.3	10.6	5.8	7.9	5.78	11.0

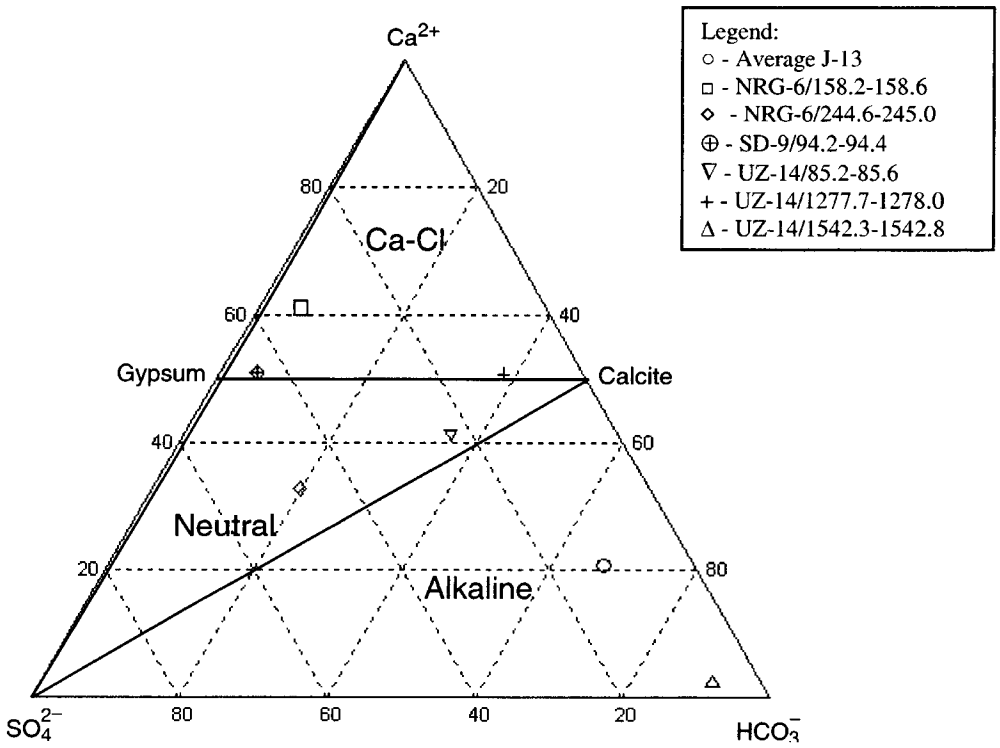

Figure 4-3. Ternary Phase Diagram of Yucca Mountain Groundwater Compositions Plotted Previously in Figure 4-1a

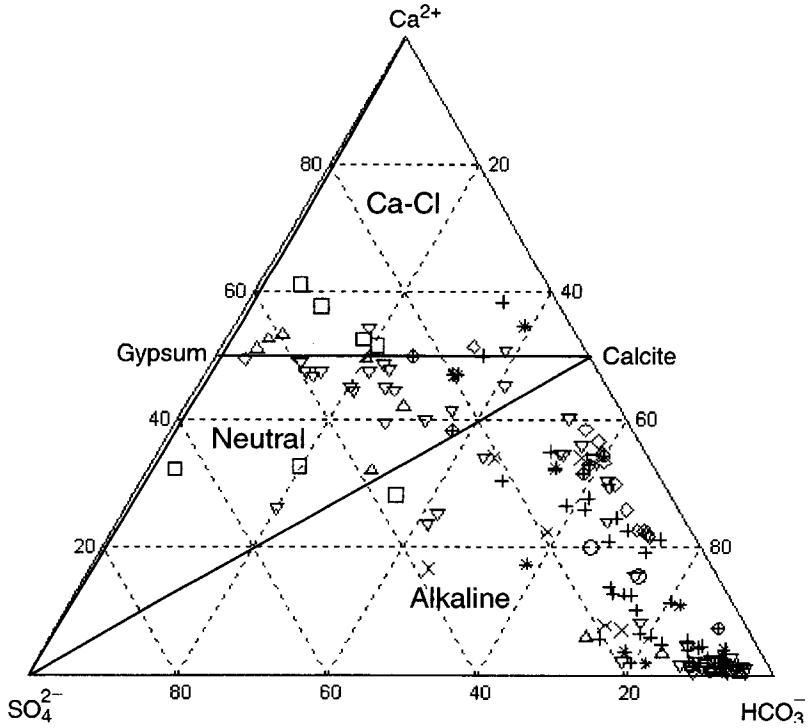

Figure 4-4. Ternary Phase Diagram of 151 Yucca Mountain Groundwater Compositions Reported by Yang, et al. (1996, 1998)

5 EXPERIMENTAL DETERMINATION OF THE DELIQUESCENCE RELATIVE HUMIDITY AND CONDUCTIVITY OF SALT MIXTURES

No literature data on the deliquescence relative humidities of salt mixtures containing Na^+, K^+, NO_3^-, and Cl^- are available; therefore, these measurements were made in this study. In addition, the relative values of ionic conductivity of various salts were determined because aqueous corrosion requires the presence of an electrolyte that is conductive to ionic species. The conductivity measurements were performed as a function of relative humidity at constant temperature. The minimum relative humidity at which conductivity starts to rise was compared to the deliquescence relative humidity of the salt. The experimental procedures and the results are presented in the following sections.

5.1 Experimental Procedures

The deliquescence relative humidity of salt mixtures was measured using a hygrometer (Model 4085CC, Control Company, Friendswood Texas, USA) with a ±1.5-percent accuracy. The test setup is shown in Figure 5-1. The measurement was conducted according to the procedures given by the relevant American Society for Testing and Materials standard (ASTM E104) (American Society for Testing and Materials, 1996). Both the glass flask containing the salt mixture and the hygrometer were placed in an oven (Model 838F, Fisher Scientific). The temperature was held constant for at least 30 minutes at the temperature of interest before each measurement was made. The temperature reading of the built-in temperature sensor of the hygrometer was recorded as the saturation temperature. During the experiment, identical glass flasks containing pure salt solutions of NaCl, $NaNO_3$, KNO_3, KCl, and $MgCl_2$ were also placed in the oven and used as controls for verifying and correcting the hygrometer readings based on their deliquescence relative humidity values published in the literature (Greenspan, 1977). The measured deliquescence relative humidities for these salts in the temperature range of 23 to 86 °C [73 to 187 °F] are compared with literature values (Greenspan, 1977) in Table 5-1.

The conductivity of the hygroscopic salts was measured using the conductivity cells illustrated in Figure 5-2. Each cell had one layer of filtration paper, with a thickness of 0.23 mm [0.0091 in], placed between two platinum electrodes. The Type A cell had a slot, with dimensions of 1.0 (thickness) × 3 (width) × 31 (length) mm [0.039 × 0.12 × 1.2 in], in which the filter paper and aqueous solution were placed. The Type B cell did not have a slot, and the filtration paper, with dimensions of 0.23 (thickness) × 26 (width) × 46 (length) mm [0.0091 × 1.0 × 1.1 in], was placed on the arched Teflon surface in contact with the electrodes. Prior to the test, the filtration paper used in both cell types was soaked in a solution that was saturated, at the testing temperature, with the salt or salt mixtures of interest. The filtration paper was used to help form an evenly distributed layer of salt deposit between the two electrodes. It was observed in preliminary tests that, if the filtration paper was not used, salt tends to form isolated clumps during crystallization, which makes the measurement of conductivity unreliable. The Type A cell was used during initial measurements, and the Type B cell was used in later measurements. The Type B cell is an improvement over the Type A cell because of its larger exposed surface area and thinner conducting layer, which allowed for quicker equilibration.

During the experiment, one or more conductivity cells were placed in a humidity chamber (Blue M Temperature/Humidity Cabinet by GS Blue M Electric). The relative humidity indicator

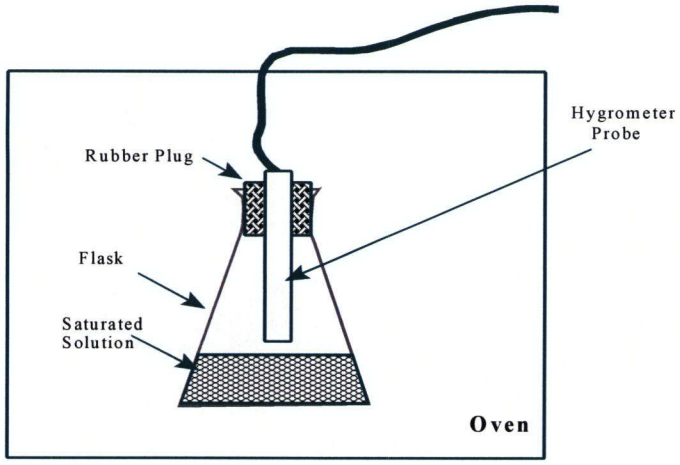

Figure 5-1. Apparatus Used for the Measurement of Deliquescence Relative Humidity

Table 5-1. Comparison Between Measured and Published Deliquescence Relative Humidity (%) for Single Salts

Salt	Temperature (°C) [°F]	Measured (%)	Published* (%)	Error (%)
NaCl	38.1 [101]	75.8	74.7	1.5
	48 [118]	76.8	74.5	3.1
	69 [156]	74.6	75.0	-0.5
$NaNO_3$	23 [73]	74.9	75.0	-0.1
	48 [118]	69.7	69.5	0.3
	69 [156]	62.7	66.2	-5.3
KNO_3	48 [118]	86.5	85.5	1.1
KCl	23 [73]	84.6	84.6	0.0
	38.1 [101]	81.7	82.6	-1.1
	48 [118]	78.3	81.5	-4.0
	69 [156]	82.0	79.6	3.0
	85.8 [186]	78.7	78.6	0.1
$MgCl_2$	23 [73]	33.9	32.8	3.5
	38.1 [101]	31.7	31.7	0.0
	48 [118]	31.0	30.7	1.1
	69 [156]	29.1	28.0	3.8
	85.8 [186]		25.0	0.4

*Greenspan, L. "Humidity Fixed Points of Binary Saturated Aqueous Solutions." *Journal of Research of the National Bureau of Standards*. Vol. 81A No. 1. pp. 89–96. 1977.

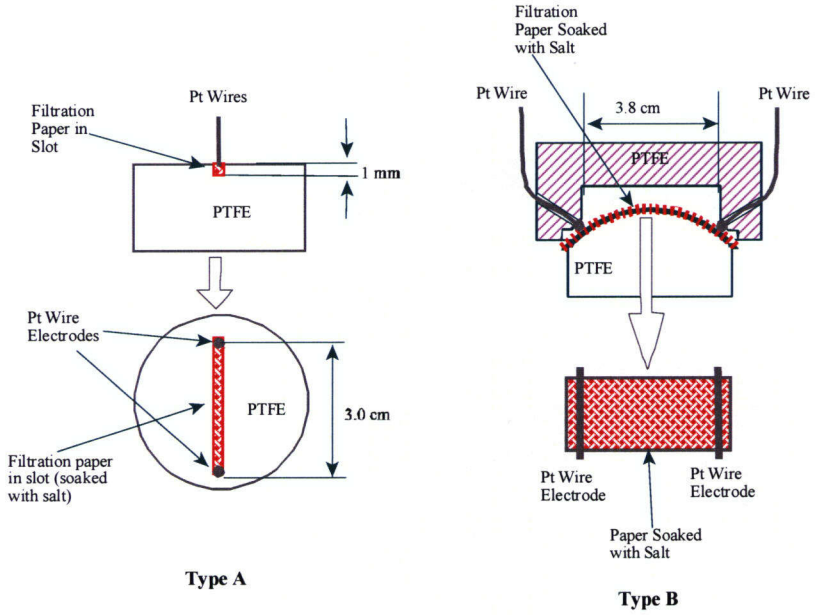

Figure 5-2. Schematic Diagrams of the Conductivity Cells Used in the Study

of the chamber was calibrated using the hygrometer previously mentioned. The relative humidity of the chamber was also cross-checked using the measured conductivities of pure salts (see the results section). An Electrochemical Interface (Model SI 1287, Solartron) and an Impedance/Gain-Phase Analyzer (Model SI 1260, Solartron) in conjunction with the Z-Plot Version 2.1 software (Scribner Associates) were used to measure the impedance between the two electrodes at a frequency of 1,000 Hz. Because the Z-Plot Version 2.1 software measures the impedance spectrum for one frequency cycle only, a graphical user interface-based Visual Basic program was developed for the experiment. The Visual Basic program activates the Z-Plot Version 2.1 impedance measurement functions at a predetermined time interval (usually 1 or 5 minutes) using the Z-Plot's Object Link and Embed feature. The Visual Basic program also displays the impedance data graphically on a computer monitor and saves the data in memory as they become available from the Z-Plot Version 2.1 program.

All solutions were prepared using 18.2 Mohm-cm deionized water and reagent grade chemicals supplied by Fisher Scientific.

5.2 Measured Deliquescence Relative Humidity of Salt Mixtures

The measured deliquescence relative humidities of salt mixtures as a function of temperature are given in Table 5-2 and plotted in Figure 5-3. For comparison, the deliquescence relative humidities of pure salts taken from the literature (Greenspan, 1977) are also presented in the figure. Figure 5-3 shows that the deliquescence relative humidities of salt mixtures containing

Table 5-2. Measured Deliquescence Relative Humidity (%) of Salt Mixtures					
Salt Mixture	Temperature (°C) [°F]				
	23.0 [73]	38.1 [101]	48.0 [118]	69.0 [156]	85.8 [186]
$NaCl+NaNO_3+KNO_3$	67.8	60.7	61.3	51.8	43.4
$NaCl+NaNO_3$	74.7	66.4	67.2	59.6	56.0
$MgCl_2+NaCl$	31.7				

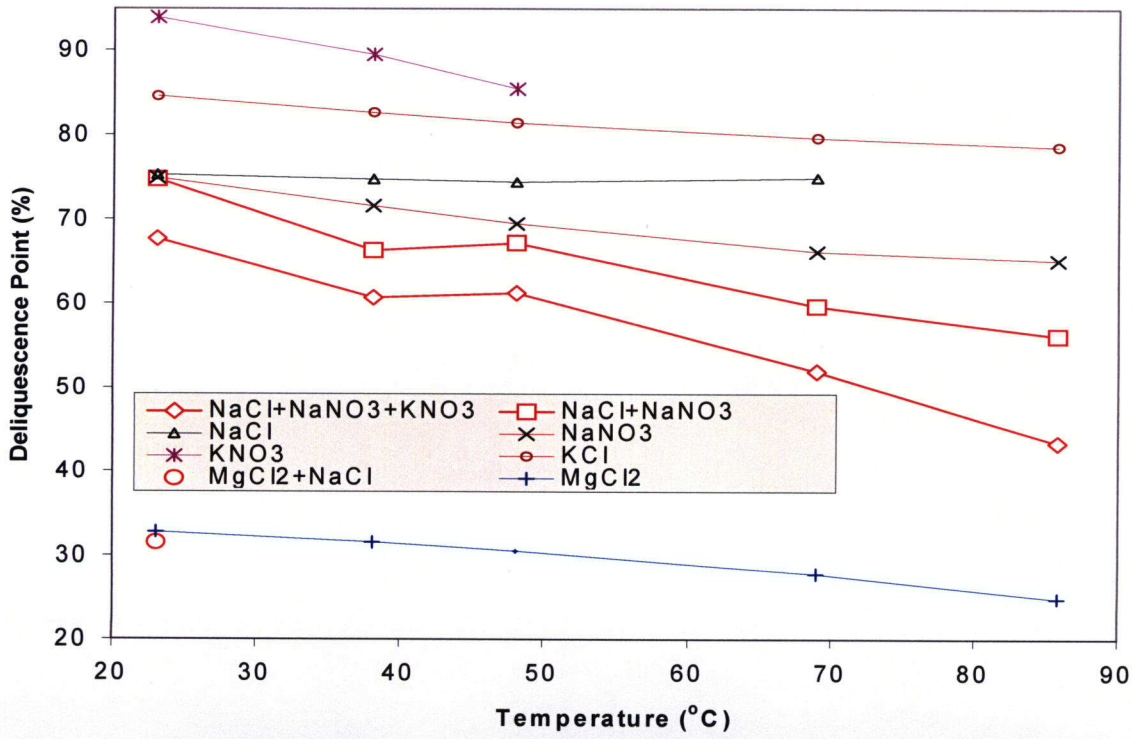

Figure 5-3. Comparison Between the Deliquescence Relative Humidities of Pure and Mixed Salts. Values for Salt Mixtures Are From This Study; Values for Pure Salts Are from Greenspan (1977).

sodium, potassium, nitrate, and chloride are significantly lower than those of the single-salt components. At a temperature of 86 °C, the lowest deliquescence relative humidity among the single salts of sodium and potassium is 65 percent (for $NaNO_3$), whereas the deliquescence relative humidity of the $NaCl+NaNO_3+KNO_3$ mixture is only 43 percent. The latter value is significantly lower than the former, which is used as the critical relative humidity for aqueous

corrosion by DOE in its analysis (CRWMS M&O, 2000a,d). The lower deliquescence relative humidity of salt mixtures measured in this study compared to single salts supports experimental data published in the literature and the results of thermodynamic calculations discussed in a preceding section. The lower deliquescence relative humidity of salt mixtures suggests that the onset of aqueous corrosion of the drip shield and waste package may be earlier and its duration may be longer than the onset and duration that are assumed based on the deliquescence relative humidity of a pure $NaNO_3$ salt. Also, because deliquescence relative humidity generally decreases with increasing temperature, a lower deliquescence relative humidity implies that formation of a corrosive brine and possible initiation of aqueous corrosion may occur at a temperature that is higher than assumed based on the deliquescence relative humidity of $NaNO_3$.

The deliquescence relative humidity of the $NaCl+NaNO_3+KNO_3$ system at 16.5 °C [61.7 °F] was reported to be 30.5 percent (Weast, 1981). This value, however, was not reproduced in this work; based on the trend shown in Figure 5-3, the deliquescence relative humidity for this mixture is likely to be 70 percent at 16.5 °C [61.7 °F]. This disagreement contrasts with the observed good agreement between all the measured pure salt deliquescence relative humidity and published data (see Table 4-1).

5.3 Measured Conductivity of Salt Deposits

Figure 5-4 shows typical responses of the impedance between two platinum electrodes measured at three frequencies to changes in relative humidity at 30 °C [86 °F]. For the measurements, the filtration paper was soaked with saturated KCl solution, and the Type A conductivity cell was used. As shown in Figure 5-4, the impedances measured at high frequencies were slightly lower than those measured at lower frequencies. Figure 5-4 also shows that when the relative humidity was low (significantly lower than the deliquescence relative humidity of the salt), the responses measured at frequencies higher than 1,000 Hz were poor, and no response at all was observed at a frequency of 100,000 Hz and low relative humidity. Therefore, 1,000 Hz was chosen as the frequency when measuring the impedance for this study.

Figure 5-5 shows the relationship between the impedance data (Figure 5-4, 1,000 Hz) and relative humidity. At relative humidities less than 65 percent, the impedance was close to 1×10^7 ohm, which is the value measured with the electrodes disconnected (i.e., the upper limit of the experimental setup measuring at a 1,000-Hz frequency). At a relative humidity close to 67 percent (or approximately 20 percent below the deliquescence relative humidity), the impedance starts to decrease and reaches 1×10^5 ohm at a relative humidity just below the deliquescence relative humidity (83 percent). When the relative humidity is slightly above the deliquescence relative humidity, the impedance decreases significantly to approximately 1×10^3 ohm.

In principle, the conductivity of the salt, λ ($ohm^{-1} \cdot m^{-1}$ or $S \cdot m^{-1}$), can be calculated according to Eqs. (5-1) and (5-2):

$$L_R = 1/Z \tag{5-1}$$

$$L = \lambda(A/l) \tag{5-2}$$

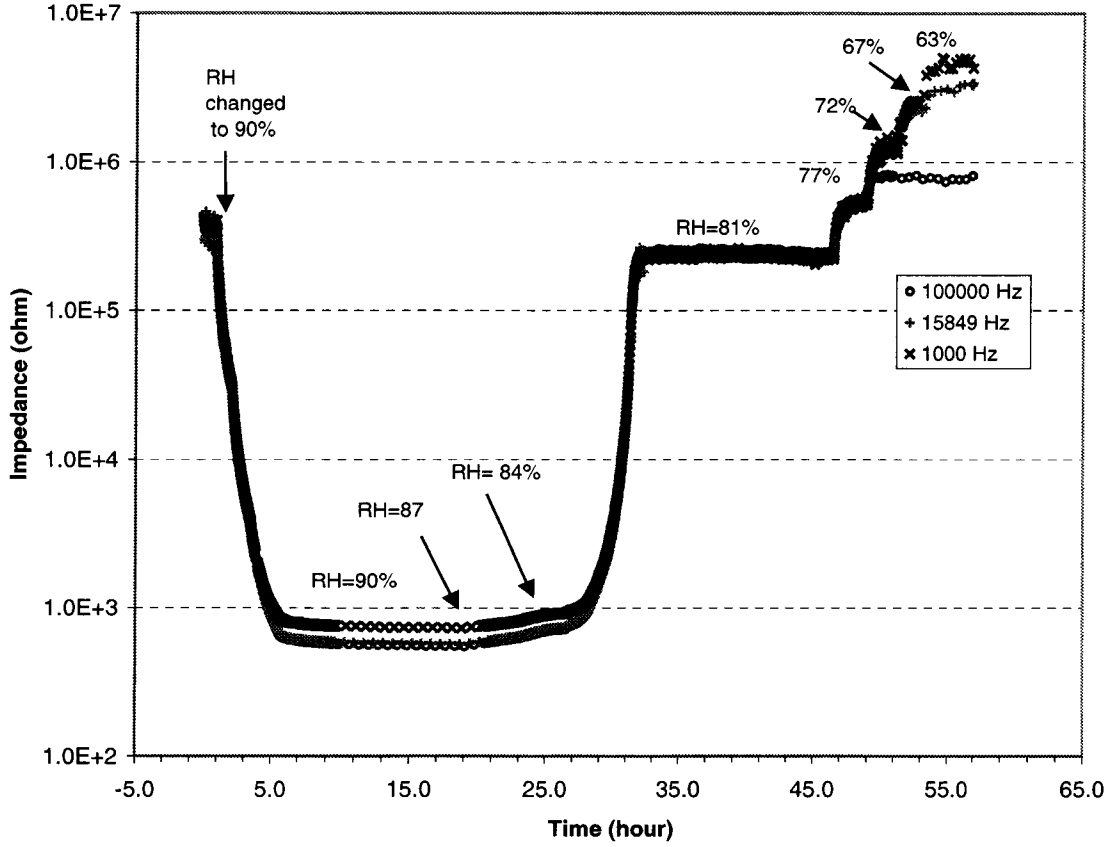

Figure 5-4. Typical Responses of Impedance Measured at Three Frequencies to Changes in Relative Humidity. The Conductivity Measurements Were Performed on Saturated KCl Solutions at 30 °C [86 °F].

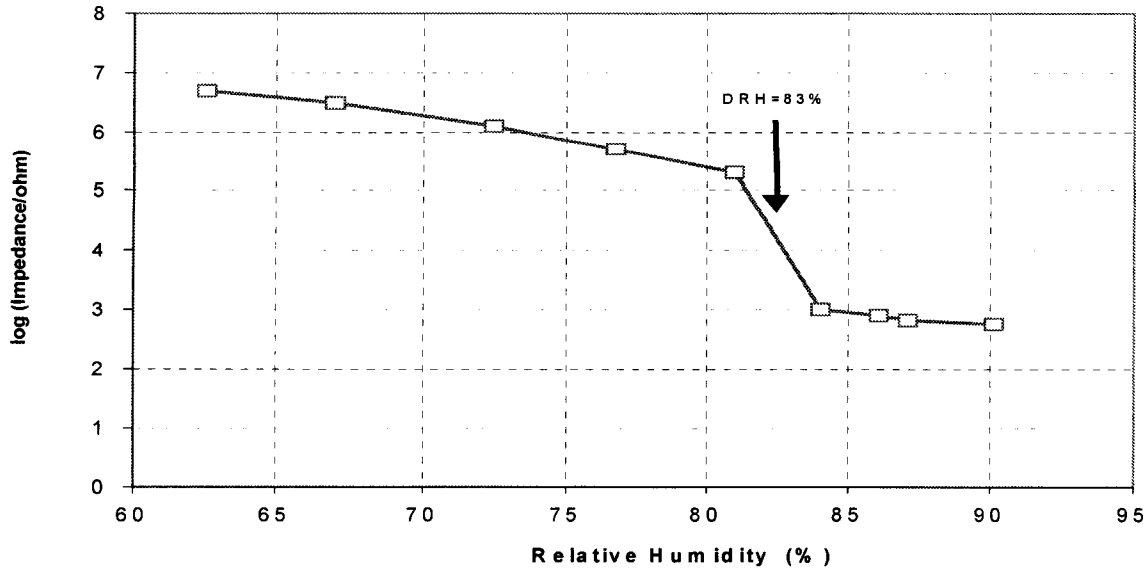

Figure 5-5. Data for KCl at 30 °C [86 °F] Showing the Typical Relationship Between Impedance and Relative Humidity.

where L is the conductance (ohm^{-1}), Z is the measured impedance (ohm), A is the cross-sectional area of the wetted filtration paper (thickness multiplied by width, m^2) and l is the distance (m) between the two electrodes. The ratio of l/A is also called the conductivity cell constant. The value of A for the filtration paper, however, is not precisely known because the conducting electrolyte layer may become thicker than the dry paper when the salt absorbs water at high relative humidities. Thus, the conductivity cell constant is not well defined. To avoid difficulties in deriving the values of conductivity, λ, the relative conductance L_R or relative conductivity λ_r of the salt is reported in this paper. The relative conductance and relative conductivity are defined as

$$L_R = L / L^o \tag{5-3}$$

$$L_R = Z^o / Z \tag{5-4}$$

and

$$\lambda_R = \lambda / \lambda^o \tag{5-5}$$

In Eqs. (5-3) through (5-5), the superscript o denotes the values of conductance, impedance, and conductivity measured at a relative humidity immediately above the deliquescence relative humidity of the salt.

Substitution of Eq. (5-2) into Eq. (5-5) yields:

$$\lambda_R = L_R \left(A^o / l^o\right)(A / l) \tag{5-6}$$

Therefore, the numerical value of the relative conductance, L_R, is identical to the relative conductivity, λ_R, if the conductivity cell constant is not affected by the relative humidity (i.e., $A/l = A^o/l^o$). In the relative humidity range below the deliquescence relative humidity, the change in the thickness of the electrolyte layer may not be significant, even though empty spaces may be formed in the pores when water evaporates at low relative humidities. Therefore, A/l may be considered constant in this range. The relative conductance may be used as an approximation of the relative conductivity, or apparent relative conductivity, for the purpose of this work.

Table 5-3 presents the measured values of impedance and conductance of KCl and $NaNO_3$ solutions at different relative humidities at 30 °C [86 °F]. Calculated values of δRH, which is the difference between the measured relative humidity and the deliquescence relative humidity of the salt, are also given in the table and are used as a normalized relative humidity. Figure 5-6 shows the relative conductance values of KCl and $NaNO_3$ as a function of the δRH. As shown in the figure, the relative conductance of KCl and $NaNO_3$ increased from approximately 2×10^{-4}, which is close to the lower detection limit of the measuring system, to about 1×10^{-2} when δRH changed from values in the range -20 to -55 percent to values approaching 0 percent. At δRHs at or just above 0 percent, the relative conductance is unity. Conductance of the salts requires the presence of water for the transport of ionic species. The

Table 5-3. Values of Impedance, Relative Conductance, and δRH^* of Salts Measured at 30 °C [86 °F] and Different Relative Humidities (RH)†

	RH (%)	Impedance (ohm)	Conductance (1/ohm)	Relative Conductance	δRH (%)
KCl DRH=83.6%‡	90.1	560	1.78×10^{-3}	1.78×10^{0}	6.5
	87.1	630	1.58×10^{-3}	1.58×10^{0}	3.5
	86.1	790	1.26×10^{-3}	1.26×10^{0}	2.5
	84.0	1000	1.00×10^{-3}	1.00×10^{0}	0.4
	80.9	200000	5.01×10^{-6}	5.01×10^{-3}	-2.7
	76.7	500000	2.00×10^{-6}	2.00×10^{-3}	-6.9
	72.5	1300000	7.94×10^{-7}	7.94×10^{-4}	-11.1
	67.0	3200000	3.16×10^{-7}	3.16×10^{-4}	-16.6
	62.6	5000000	2.00×10^{-7}	2.00×10^{-4}	-21.0
$NaNO_3$ DRH=73.1%‡	89.1	1000	1.00×10^{-3}	2.00×10^{0}	16
	76.7	2000	5.01×10^{-4}	1.00×10^{0}	3.6
	72.5	400000	2.51×10^{-6}	5.01×10^{-3}	-0.6
	68.1	1000000	1.00×10^{-6}	2.00×10^{-3}	-5.0
	54.6	3500000	2.82×10^{-7}	5.62×10^{-4}	-18.5
	20.5	7900000	1.26×10^{-7}	2.51×10^{-4}	-52.6

*difference between the measured relative humidity and the deliquescence relative humidity of the salt
†Cell: Type A.
‡Published data (Greenspan, L. "Humidity Fixed Points of Binary Saturated Aqueous Solutions." *Journal of Research of the National Bureau of Standards*. Vol. 81A No. 1. pp. 89–96. 1977).

increase in the conductance or conductivity of the salts at relative humidities lower than their deliquescence relative humidities (at negative δRH values) implies that adsorption of water on salt particles initiates at relative humidities lower than the deliquescence relative humidity. This observation is consistent with previous findings (Cohen, et al., 1987b; Ge, et al., 1998; Vogt and Finlayson-Pitts, 1994) on the adsorption of water on salt particles. Vogt and Finlayson-Pitts (1994), using diffuse reflectance infrared Fourier transform spectrometry, observed that significant amounts of water reside on the surface of a pure NaCl aerosol surface at a relative humidity of 53.8 percent, far below its deliquescence relative humidity of 75.7 percent.

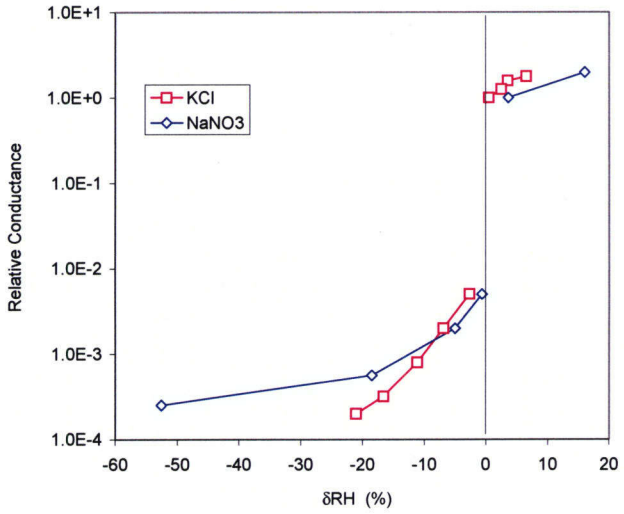

Figure 5-6. Measured Relative Conductance of KCl and $NaNO_3$ at 30 °C [86 °F] as a Function of δRH , Which Is the Difference Between the Measured Relative Humidity and the Deliquescence Relative Humidity of the Salt. Type A Cell Was Used.

Additional experiments at 50 °C [122 °F] were conducted in this study, and the data are presented in Table 5-4 and Figure 5-7. The variations in the relative conductance of the different salt and salt mixtures at a given δRH are probably caused by variations in the particle size, porosity, surface roughness, and hydrophilic properties of the salts. Although not a sufficient condition, the presence of water is a necessary condition for aqueous corrosion to take place. It is not known from the experiments how much water was adsorbed at the time conductivity started to increase. It has been reported that aqueous films thicker than three monolayers possess properties close to those of bulk water (Leygraf and Graedel, 2000). The increase in relative conductance as shown in Figures 5-6 and 5-7 also implies that aqueous corrosion might take place at a relative humidity 20 percent lower than the deliquescence relative humidity of the salt deposits.

Simulation by DOE (CRWMS M&O, 2000c) shows that after emplacement of nuclear waste packages in the proposed repository, the temperature of the waste package may increase to approximately 100 °C [212 °F] and then decrease during the ventilation period. After closure of the drift, the temperature of the waste package again may increase sharply to 160 °C [320 °F]. The minimum relative humidity that corresponds to the 160 °C [320 °F] peak temperature is approximately 20 percent. According to the DOE salt/precipitate analysis, it is likely that the salt deposit on the waste package and drip shield would be a mixture containing NaCl, $NaNO_3$, and KNO_3 (CRWMS M&O, 2000a). Because the deliquescence relative humidity of this mixture is expected to be significantly lower than the deliquescence relative humidity of pure $NaNO_3$ salt

Table 5-4. Values of Impedance, Relative Conductance, and δRH^* of Salts Measured at 50 °C [122 °F] and Different Relative Humidities (RH)					
	RH (%)	**Impedance (ohm)**	**Conductance (ohm^{-1})**	**Relative Conductance**	**δRH (%)**
KNO_3–NaCl, DRH=60%	42.0	800000	1.25×10^{-6}	3.12×10^{-4}	-18.0
	42.0	1000000	1.00×10^{-6}	2.50×10^{-4}	-18.0
	44.0	350000	2.86×10^{-6}	7.14×10^{-4}	-16.0
	51.0	250000	4.00×10^{-6}	1.00×10^{-3}	-9.0
	54.0	35000	2.86×10^{-5}	7.14×10^{-3}	-6.0
	58.0	25000	4.00×10^{-5}	1.00×10^{-2}	-2.0
	62.0	250	4.00×10^{-3}	1.00×10^{0}	2.0
	65.0	210	4.76×10^{-3}	1.19×10^{0}	5.0
	73.0	220	4.55×10^{-3}	1.14×10^{0}	13.0
	86.0	250	4.00×10^{-3}	1.00×10^{0}	26.0
$NaNO_3$, DRH=69.04%†	42.0	5000000	2.00×10^{-7}	7.00×10^{-5}	-27.0
	42.0	1800000	5.56×10^{-7}	1.94×10^{-4}	-27.0
	44.0	1800000	5.56×10^{-7}	1.94×10^{-4}	-25.0
	51.0	800000	1.25×10^{-6}	4.37×10^{-4}	-18.0
	54.0	200000	5.00×10^{-6}	1.75×10^{-3}	-15.0
	58.0	150000	6.67×10^{-6}	2.33×10^{-3}	-11.0
	61.0	100000	1.00×10^{-5}	3.50×10^{-3}	-8.0
	62.0	80000	1.25×10^{-5}	4.38×10^{-3}	-7.0
	65.0	25000	4.00×10^{-5}	1.40×10^{-2}	-4.0
	73.0	350	2.86×10^{-3}	1.00×10^{0}	4.0
	86.0	350	2.86×10^{-3}	1.00×10^{0}	17.0

Table 5-4. Values of Impedance, Relative Conductance, and δRH * of Salts Measured at 50 °C [122 °F] and Different Relative Humidities (RH) (continued)					
	RH (%)	Impedance (ohm)	Conductance (ohm^{-1})	Relative Conductance	δRH (%)
$NaNO_3$–NaCl DRH=66%	43.0	10000000	1.00×10^{-7}	3.20×10^{-5}	-23.0
	50.0	730000	1.37×10^{-6}	4.38×10^{-4}	-16.0
	55.0	350000	2.86×10^{-6}	9.14×10^{-4}	-11.0
	60.0	35000	2.86×10^{-5}	9.14×10^{-3}	-6.0
	63.0	20000	5.00×10^{-5}	1.60×10^{-2}	-3.0
	66.0	320	3.13×10^{-3}	1.00×10^{0}	0.0
	79.0	320	3.13×10^{-3}	1.00×10^{0}	13.0
$NaNO_3$–KNO_3–NaCl DRH=60%	43.0	900000	1.11×10^{-6}	3.33×10^{-4}	-17.0
	50.0	200000	5.00×10^{-6}	1.50×10^{-3}	-10.0
	55.0	75000	1.33×10^{-5}	4.00×10^{-3}	-5.0
	60.0	300	3.33×10^{-3}	1.00×10^{0}	0.0
	63.0	200	5.00×10^{-3}	1.50×10^{0}	3.0
	66.0	250	4.00×10^{-3}	1.20×10^{0}	6.0
	66.0	200	5.00×10^{-3}	1.50×10^{0}	6.0
	79.0	250	4.00×10^{-3}	1.20×10^{0}	19.0
$MgCl_2$–NaCl DRH = 30.2%	20.0	4000000	2.50×10^{-7}	1.53×10^{-4}	-10.2
	24.0	1300000	7.69×10^{-7}	4.69×10^{-4}	-6.2
	27.0	350000	2.86×10^{-6}	1.74×10^{-3}	-3.2
	27.0	400000	2.50×10^{-6}	1.53×10^{-3}	-3.2
	29.0	200000	5.00×10^{-6}	3.05×10^{-3}	-1.2
	30.0	100000	1.00×10^{-5}	6.10×10^{-3}	-0.2
	31.0	610	1.64×10^{-3}	1.00×10^{0}	0.8
	31.0	650	1.54×10^{-3}	9.38×10^{-1}	0.8
	33.0	570	1.75×10^{-3}	1.07×10^{0}	2.8
	34.0	600	1.67×10^{-3}	1.02×10^{0}	3.8
	36.5	540	1.85×10^{-3}	1.13×10^{0}	6.3

Table 5-4. Values of Impedance, Relative Conductance, and δRH of Salts Measured at 50 °C [122 °F] and Different Relative Humidities (RH) (continued)					
	RH (%)	Impedance (ohm)	Conductance (ohm^{-1})	Relative Conductance	δRH (%)
$MgCl_2$–NaCl DRH = 30.2%	36.5	530	1.89×10^{-3}	1.15×10^{0}	6.3
$MgCl_2$–NaCl DRH = 30.6%	20.0	3000000	3.33×10^{-7}	2.17×10^{-4}	-10.6
	24.0	800000	1.25×10^{-6}	8.12×10^{-4}	-6.6
	27.0	200000	5.00×10^{-6}	3.25×10^{-3}	-3.6
	27.0	250000	4.00×10^{-6}	2.60×10^{-3}	-3.6
	29.0	160000	6.25×10^{-6}	4.06×10^{-3}	-1.6
	30.0	130000	7.69×10^{-6}	5.00×10^{-3}	-0.6
	31.0	650	1.54×10^{-3}	1.00×10^{0}	0.4
	31.0	700	1.43×10^{-3}	9.29×10^{-1}	0.4
	33.0	610	1.64×10^{-3}	1.07×10^{0}	2.4
	34.0	570	1.75×10^{-3}	1.14×10^{0}	3.4
	36.5	580	1.72×10^{-3}	1.12×10^{0}	5.9
	36.5	580	1.72×10^{-3}	1.12×10^{0}	5.9
KNO_3 DRH = 84.8%	57.0	2000000	5.01×10^{-7}	1.35×10^{-4}	-27.8
	64.0	600000	1.66×10^{-6}	4.47×10^{-4}	-20.8
	64.0	790000	1.26×10^{-6}	3.39×10^{-4}	-20.8
	68.0	270000	3.72×10^{-6}	1.00×10^{-3}	-16.8
	68.0	500000	2.00×10^{-6}	5.37×10^{-4}	-16.8
	70.0	400000	2.51×10^{-6}	6.76×10^{-4}	-14.8
	72.0	250000	3.98×10^{-6}	1.07×10^{-3}	-12.8
	72.0	400000	2.51×10^{-6}	6.76×10^{-4}	-12.8
	75.0	300000	3.31×10^{-6}	8.91×10^{-4}	-9.8
	82.0	100000	1.00×10^{-5}	2.69×10^{-3}	-2.8
	89.0	270	3.72×10^{-3}	1.00×10^{0}	4.2
	99.0	280	3.55×10^{-3}	9.55×10^{-1}	14.2

Table 5-4. Values of Impedance, Relative Conductance, and δRH * of Salts Measured at 50 °C [122 °F] and Different Relative Humidities (RH) (continued)

	RH (%)	Impedance (ohm)	Conductance (ohm^{-1})	Relative Conductance	δRH (%)
KCl DRH = 81.2%	57.0	1000000	1.00×10^{-6}	3.47×10^{-4}	-24.2
	64.0	200000	5.01×10^{-6}	1.74×10^{-3}	-17.2
	64.0	450000	2.24×10^{-6}	7.76×10^{-4}	-17.2
	68.0	95000	1.05×10^{-5}	3.63×10^{-3}	-13.2
	68.0	250000	3.98×10^{-6}	1.38×10^{-3}	-13.2
	70.0	120000	8.32×10^{-6}	2.88×10^{-3}	-11.2
	82.0	350	2.88×10^{-3}	1.00×10^{0}	0.8
	89.0	220	4.57×10^{-3}	1.58×10^{0}	7.8
	99.0	1000	1.00×10^{-3}	3.47×10^{-1}	17.8

*δRH—difference between the measured relative humidity and the deliquescence relative humidity of the salt
†Published data (Greenspan, L. "Humidity Fixed Points of Binary Saturated Aqueous Solutions." *Journal of Research of the National Bureau of Standards*. Vol. 81A No. 1. pp. 89–96. 1977.); Cell: Type B

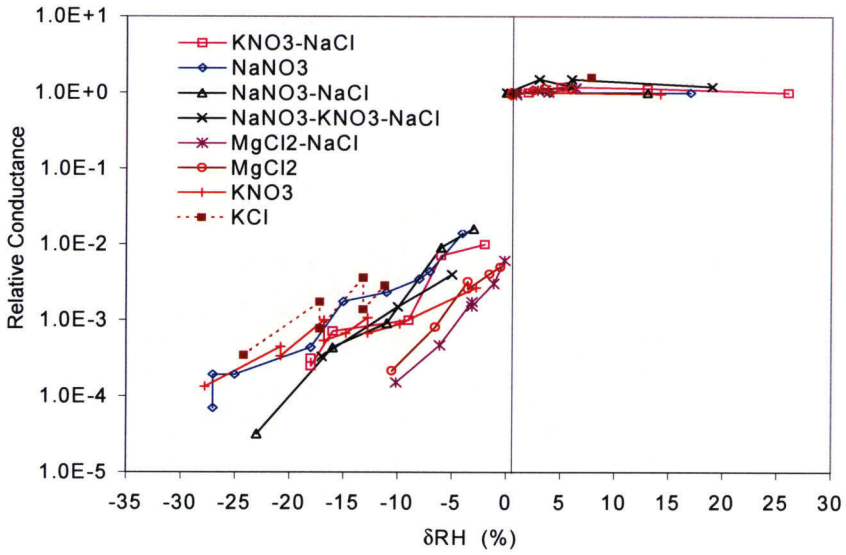

Figure 5-7. Relative Conductance of Salts Measured at 50 °C [122 °F] as a Function of δRH , the Difference Between the Relative Humidity and the Deliquescence Relative Humidity. Note, Type B Cell Was Used.

and if aqueous corrosion starts at relative humidities 20 percent below the deliquescence relative humidity, aqueous corrosion may take place during the entire emplacement period. Therefore, the critical relative humidity used by DOE may not be realistic and uncertainties in this parameter should be incorporated in performance assessments.

6 CONCLUSIONS

The results of thermodynamic calculations and experimental measurements conducted in this study support literature data that show the deliquescence points of salt mixtures are lower than those of individual salts. Thermodynamic analyses indicate that mixtures comprising NaCl and KCl salts have higher deliquescence points than pure $NaNO_3$, but deliquescence relative humidity measurements show that mixtures of NaCl, $NaNO_3$, and KNO_3 have significantly lower mutual deliquescence relative humidity than pure $NaNO_3$. Additional thermodynamic analyses and experimental measurements show that mixtures containing magnesium and calcium have much lower mutual deliquescence relative humidities than pure $NaNO_3$. Thus, the $NaNO_3$-based deliquescence relative humidity used by DOE in its analysis of the chemical environment on the surface of drip shields and waste packages does not bound the deliquescence points of salt mixtures expected to form on those surfaces.

Thermodynamic simulations show that some Yucca Mountain unsaturated zone groundwaters could evolve through evaporation into brines characterized by very low mutual deliquescence relative humidity, high chloride concentration, and low concentrations of anions, such as nitrate and sulfate, that could mitigate against the chloride-enhanced corrosion of the waste package. Qualitative information derived from the chemical divide approach, however, suggests that only approximately 8 percent of the reported unsaturated zone groundwater composition would evolve into that type of brine. The other 92 percent of the groundwater compositions considered in the analysis would form brines that have lower deliquescence relative humidity than pure $NaNO_3$, but not as low as the other type. The thermodynamic simulations also show that if fluoride ions are present in the groundwater, evaporative concentration would lead to fluoride concentrations that are above the threshold for accelerated corrosion of the titanium drip shield.

The results of relative conductivity measurements show that as the relative humidity increases, the conductivity of a dry salt or salt mixture starts to increase at a humidity value significantly lower than the deliquescence relative humidity of the salt or salt mixture. This increase in conductivity implies that initiation of drip shield or waste package aqueous corrosion may occur at a relative humidity significantly lower than the deliquescence relative humidity of the salt mixture deposited on them. The effect of a lower deliquescence point on institution and rate of corrosion processes need to be included in performance assessment.

The independent analyses presented in this report support the NRC risk-informed approach in several ways. Most importantly, the results described in this report indicate that extreme chemical environments are plausible on the drip shield and waste package surfaces in response to in-drift evaporation and salt formation processes, and these chemical environments might adversely impact drip shield and waste package lifetimes. An important implication of this work is that in-drift processes should be considered explicitly in performance assessment calculations. Container Life and Source Term and Evolution of the Near-Field Environment staffs are utilizing data and insights described in this report to include an in-drift chemistry abstraction for the NRC and CNWRA Total-system Performance Assessment Version 5.0 code. This effort will result in a more realistic, quantifiable evaluation of the risk insights associated with drip shield and waste package lifetimes. The results of this study are also being used to evaluate DOE work such as the anticipated responses to seven Evolution of the Near-Field

Environment Technical Exchange agreements (i.e., ENFE 2.04, 2.06, 2.09, 2.10, 2.14, 2.15, and 2.17) that are directly related to the in-drift chemical environment.[1]

[1]Reamer, C.W. "U.S. Nuclear Regulatory Commission/U.S. Department of Energy Technical Exchange and Management Meeting on the Evolution of the Near-Field Environment (January 9–11, 2000). Letter to D.R. Williams, DOE. Washington, DC: NRC. 2001.

7 REFERENCES

American Standard for Testing Materials. "Standard Practice for Maintaining Constant Relative Humidity by Means of Aqueous solutions Standard." West Conshohocken, Pennsylvania. ASTM Designation E104–85 (Reapproved 1996). 1996.

Bechtel SAIC Company, LLC. "FY01 Supplemental Science and Performance Analyses." Vol 1: Scientific Bases and Analyses. TDR–MGR–MD–000007. Rev. 00, ICN 01. Las Vegas, Nevada: Bechtel SAIC Company, LLC. 2001.

Bromley, L.A. "Approximate Individual Ion Values of β (or B) in Extended Debye-Huckel Theory for Uni-Univalent Aqueous Solutions at 298.15 K." *Journal of Chemical Thermodynamics.* Vol. 4. pp. 669–673. 1972.

Brossia, C.S. and G.A. Cragnolino. "Effects of Environmental and Metallurgical Conditions on the Passive and Localized Dissolution of Ti–0.15Pd." *Corrosion.* Vol. 57. pp. 68–776. 2001.

Browning, L., W.M. Murphy, B.W. Leslie, and W.L. Dam. "Thermodynamic Interpretations of Chemical Analyses of Unsaturated Zone Water from Yucca Mountain, Nevada." *Scientific Basis for Nuclear Waste Management XXIII.* R. Smith and D. Shoesmith, eds. Symposium Proceedings 663. Warrendale, Pennsylvania: Materials Research Society. pp. 237–242. 2000.

Cohen, M.D., R.C. Flagan, and J.H. Seinfeld. "Studies of Concentrated Electrolyte Solutions Using the Electrodynamic Balance. 1: Water Activities for Single-Electrolyte Solutions." *Journal of Physical Chemistry.* Vol. 91. pp. 4,563–4,574. 1987a.

Cohen, M.D., R.C. Flagan, and J.H. Seinfeld. "Studies of Concentrated Electrolyte Solutions Using the Electrodynamic Balance. 2: Water Activities for Mixed-Electrolyte Solutions." *Journal of Physical Chemistry.* Vol. 91. pp. 4,575–4,582. 1987b.

CRWMS M&O. "Geochemistry: Book 3–Section 6 of Yucca Mountain Site Description." B00000000–01717–5700–00019. Revision 00. Las Vegas, Nevada: CRWMS M&O. 1998.

———. "Environment on the Surfaces of the Drip Shield and Waste Package Outer Barrier." ANL–EBS–MD–000001. Revision 00. Las Vegas, Nevada: CRWMS M&O. 2000a.

———. "Repository Safety Strategy: Plan to Prepare the Postclosure Safety Case to Support Yucca Mountain Site Recommendation and Licensing Considerations." TDR–WIS–RL–000001 Revision 03. Las Vegas, Nevada. CRWMS M&O. 2000b.

———. "Total System Performance Assessment for the Site Recommendation." TDR–WIS–PA–000001. Revision 00, ICN 01. Las Vegas, Nevada: CRWMS M&O. 2000c.

———. "Waste Package Degradation Process Model Report." TDR–WIS–MD–000002. Revision 00. Las Vegas, Nevada: CRWMS M&O. 2000d.

Cragnolino, G.A., D.S. Dunn, and Y.-M. Pan. "Localized Corrosion Susceptibility of Alloy 22 as a Waste Package Container Material." Scientific Basis for Nuclear Waste Management XXV (abstract). November 26–30, 2001. Boston, Massachusetts. Materials Research Society Fall Meeting. 2001.

DOE. "Yucca Mountain Science and Engineering Report." DOE/RW–0539. Washington, DC: DOE, Office of Civilian Radioactive Waste Management. 2000.

Ge, Z., A.S. Wexler, and M.V. Johnston. "Deliquescence behavior of multicomponent aerosols." *Journal Physical of Chemistry, A.*" Vol. 102. pp173–180. 1998.

Greenspan, L. "Humidity Fixed Points of Binary Saturated Aqueous Solutions." *Journal of Research of the National Bureau of Standards.* Vol. 81A No. 1. pp. 89–96. 1977.

Hardie, L.A. and H.P. Eugster. "The Revolution of Closed-Basin Brines." *Mineralogical Society of America.* Special Paper, 3. pp. 273–290. 1970.

Harrar, J.E., J.F. Carley, W.F. Isherwood, and E. Raber. "Report of the Committee to Review the Use of J–13 Well Water in Nevada Nuclear Waste Storage Investigations." UCID–21867. Livermore, California: Lawrence Livermore National Laboratory. 1990.

Helgeson, H.C., D.H. Kirkham, and G.C. Flowers. "Theoretical Prediction of the Thermodynamic Behavior of Aqueous Electrolytes at High Pressures and Temperatures. IV. Calculation of Activity Coefficients, Osmotic Coefficients, and Apparent Molal and Standard and Relative Partial Molal Properties to 600 °C and 5 kb." *American Journal of Science.* Vol. 281. pp. 1,249–1,516. 1981.

Leygraf, C. and T. Graedel. *Atmospheric Corrosion.* New York City, New York. Wiley Interscience. 2000.

Lide, D.R., ed. *CRC Handbook of Chemistry and Physics.* Boca Raton, Florida: CRC Press. 2001.

Pabalan, R.T. "Software Validation Report for SOLCALC, Version 1.0." Letter Report. San Antonio, Texas: CNWRA. 2002.

Pabalan, R.T. and K.S. Pitzer. "Thermodynamics of Concentrated Electrolyte Mixtures and the Prediction of Mineral Solubilities to High Temperatures for Mixtures in the System Na-K-Mg-Cl-SO_4-OH-H_2O." *Geochimica et Cosmochimca Acta.* Vol. 51. pp. 2,429–2,443. 1987.

Pabalan, R.T. and K.S. Pitzer. "Prediction of High-Temperature Thermodynamic Properties of Mixed Electrolyte Solutions Including Solubility Equilibria, Vapor Pressure Depression, and Boiling Point Elevation." Proceedings: 1987 Symposium on Chemistry in High-Temperature Water. R.M. Izatt, J.L. Oscarson, and G.C. Lindh, eds. Palo Alto, California: Electric Power Research Institute. pp. D4f-1–D4f-13. 1990.

Pabalan, R.T. and K.S. Pitzer. "Mineral Solubilities in Electrolyte Solutions." *Activity Coefficients in Electrolyte Solutions.* K.S. Pitzer editor. Boca Raton, Florida: CRC Press. pp. 435–490. 1991.

Painter, S., C. Manepally, and D.L. Hughson. "Evaluation of U.S. Department of Energy Thermohydrologic Data and Modeling Status Report." Letter Report. San Antonio, Texas: CNWRA. 2001.

Pilinis, C. "Modeling Atmospheric Aerosols Using Thermodynamic Arguments—A Review." *Global Nest.* Vol. 1. pp. 5–13. 1999.

Pitzer, K.S. "Thermodynamics of electrolytes, 1: *Theoretical basis and general equations.*" *Journal of Physical Chemistry.* Vol. 77. 268–277. 1973.

Pitzer, K.S. "Ion Interaction Approach: Theory and Data Correlation." *Activity Coefficients in Electrolyte Solutions.*" K.S. Pitzer editor. Boca Raton, Florida: CRC Press. pp. 75–153. 1991.

Rosenberg, N.D., K.G. Knauss, and M.J. Dibley. "Evaporation of J–13 Water: Laboratory Experiments and Geochemical Modeling." UCRL–ID–134852. Livermore, California: Lawrence Livermore National Laboratory. 1999.

Spencer, R.J. "Sulfate Minerals in Evaporite Deposits." *Reviews in Mineralogy and Geochemistry.* Vol. 40. pp. 173–192. 2000.

Tang, I.N. and H.R. Munkelwitz. "Composition and Temperature Dependence of the Deliquescence Properties of Hygroscopic Aerosols." *Atmospheric Environment.* Vol. 27A, No.4. pp. 467–473. 1993.

Vogt, R. and B.J. Finlayson-Pitts. "A Diffuse Reflectance Infrared Fourier Transform Spectroscopic Study of the Surface Reaction of NaCl with Gaseous NO_2 and HNO_3." *A Journal of Physical Chemistry.* Vol. 98. pp. 3,747–3,755. 1994.

Weast, R.C., ed. *CRC Handbook of Chemistry and Physics.* Boca Raton, Florida: CRC Press. p. E-46. 1981.

Wexler, A.S. and J.H. Seinfeld. "Second-Generation Inorganic Aerosol Model." Atmospheric Environment. Vol. 25A. pp. 2,731–2,748. 1991.

Wolery, T.J. "EQ3NR, A Computer Program for Geochemical Aqueous Speciation-Solubility Calculations: Theoretical Manual, User's Guide, and Related Documentation (Version 7.0) Part III." UCRL–MA–110662. Livermore, California: Lawrence Livermore National Laboratory. 1992.

Yang, I.C., G.W. Rattray, and Y. Pei. "Interpretation of Chemical and Isotopic Data from Boreholes in the Unsaturated Zone at Yucca Mountain, Nevada." Water-Resources Investigations Report 96-4058. Denver, Colorado: U.S. Geological Survey. 1996.

Yang, I.C., P. Yu, G.W. Rattray, J.S. Ferarese, and J.N. Ryan. "Hydrochemical Investigations in Characterizing the Unsaturated Zone at Yucca Mountain, Nevada." Water-Resources Investigations Report 98-4132. Denver, Colorado: U.S. Geological Survey. 1998.

Yang, L., R.T. Pabalan, and L. Browning. "Experimental Determination of the Deliquescence Relative Humidity and Conductivity of Multicomponent Salt Mixtures." Symposium on the Scientific Basis for Nuclear Waste Management XXV (abstract). November 26–30, 2001. Boston, Massachusetts. Materials Research Society Fall Meeting. 2001.